Interference and fringe pattern demodulation

Pascal Picart

02.05.2024

Table des matières

I.Présentation

Module :

Interference and Diffraction

Auteur(s) :

Pascal Picart[1] - ENSIM – Le Mans Université

Résumé :

Presentation of techniques for extracting the optical phase of interference signal

Mots-clés :

Interference, Optical phase, Phase shifting, Phase modulation, Interferometry

Pré-requis :

physical optics, signal processing, uncertainty

Objectif(s) pédagogique(s) :

Understand the methods of processing
Implement the techniques for extracting the optical phase of interference signal

Plan du cours :

- Introduction
- Principle of phase demodulation
- Phase demodulation without a spatial carrrier
- Phase demodulation with spatial carrier

Conception & production :

Le Mans Université

Licence :

1 - pascal.picart@univ-lemans.fr
2 - http://www.gnu.org/licenses/fdl.txt

II.Cours

A large number of optical measurement techniques rely on the interference phenomenon, which encodes the measured physical quantity into the phase of a periodic signal. The bidimensional interferometric signal which is registered via an image sensor is called fringe pattern. Fringe patterns usually appear as stripes, alternatively bright or dark, which represent the contour lines of the measured physical quantity. The mathematical formulation of this interference field can be defined using the spatial coordinates (x, y, z) and the temporal coordinate t. We can write :

$$I(x, y, z, t) = I_0(x, y, z, t)[1 + m(x, y, z, t) f(\Delta\varphi(x, y, z, t))]$$

where :

$I_0(x, y, z, t)$, is average value of the signal,

$m(x, y, z, t)$, is the fringe pattern modulation (contrast),

$\Delta\varphi(x, y, z, t)$, is the optical phase encoding the physical quantity measured in the experiment,

$f(...)$, is a function defining the fringe pattern profile.

The function $f(...)$ can have a sinusoidal shape (for interferences between two waves), a sinusoidal shape with higher harmonics, a Lorentzian shape (for overexposed interferences), a rectangular shape (for interferences with grids), or a trapezoidal shape (for multiple interferences with grids).

The periodicity of the fringe pattern, however it was generated, incites us to write the signal using a harmonic formulation:

$$I(x, y, z, t) = a(x, y, z, t) + \sum_{n=1}^{\infty} b_n(x, y, z, t)\cos(n\Delta\varphi(x, y, z, t))$$

where $a(x, y, z, t)$ is the average signal (background) and $b_n(x, y, z, t)$ is the amplitude of the harmonic of order n.

On a pure metrological point of view, the optical techniques for which the useful signal is a fringe pattern constitute powerful measurement tools because they give instantaneous spatial information, contrary to many other techniques which give an information at a single spatial point, or possibly at an array of points after scanning (in general a long and tedious process); moreover, these optical techniques encode information of a certain magnitude (the measured physical quantity), usually in a bi or tri-dimensional space.

In most cases, this encoding process can be seen as a double application which, on one hand, assigns a certain value of the signal to each value of the measured physical quantity, and, on the other hand, assigns to each space point the corresponding interferometric value. The first assignment of corresponding values is done by the phase $\Delta\varphi(x, y, z, t)$ via a relation specific to each situation. The second assignment is, as the first one, intimately related to the optical technique used for the measurement, and is established by the analysis of image formation in the optical system used for the measurement.

Consequently, the fringe pattern gives information in which the fringes constitute the lines of equal variation of the optical phase. For most applications, the optical system is designed such that the mean background $I_0(x, y, z, t)$ and the contrast $\mathrm{m}(x, y, z, t)$ stay almost constant across the field of measurement. However, some methods (such as interferometry) inherently lead to non-constant $I_0(x, y, z, t)$ and $\mathrm{m}(x, y, z, t)$. This is why technical development, stimulated by an increasing demand in precision, rapidity, and automation, contributed to the development of methods for which a precise interpolation between extreme values hides the rapid variations of $I_0(x, y, z, t)$ and $\mathrm{m}(x, y, z, t)$, eliminates the ambiguities on the measurement of $\Delta\varphi(x, y, z, t)$ and allows a simple analysis even by non-specialists of the topic.

The analysis of the fringe patterns is the purpose of this lesson. Generally, it is done by completing the following steps:

- **Determination of the optical phase** ; it consists in obtaining the spatial distribution of the optical phase $\Delta\varphi$, traditionally called phase map, starting from one or several interference patterns associated to the same measured physical quantity.
- **Phase unwrapping** ; in the vast majority of cases, the previous step gives a phase distribution that is only known modulo 2π ; determining the interference order k i.e. the term $\Delta\varphi = 2k\pi$; is necessary to obtain phase continuity; this is called phase unwrapping.
- **Suppression of unwanted terms** ; the parasite terms that may have been introduced in the phase and that do not carry any useful information on the measured physical quantity must be suppressed using a least square approximation or any other suitable method; these terms may have been introduced during fringe pattern formation and/or during phase determination.
- **Rescaling the results** ; in most cases, a correct presentation of the results requires the knowledge of the relationship between the values of the measured physical data and the coordinate system of the space where it is defined (this relationship can take the form of a mathematical expression, a table, a graph, a relation between gray levels or color codes...); this step thus requires the knowledge of the relationship between, and one hand, the phase $\Delta\varphi$and the magnitude of the measured physical quantity, and, on the other hand, between the bidimensional space of the phase map and the spatial domain of the measured physical quantity; of course, these relationships depend on the method used.
- **Readjustment** ; in some cases, it is necessary to confront the experiment with an analytical model; this leads to a readjustment between the numerical simulation which is supposed to describe the behavior of the analyzed element and the measurement which brings an objective analysis of this behavior.

Once the readjustment has been done, the analysis process can be regarded as complete; however, only the first three steps are usually completed. The first step, phase determination, is a common step independent from the other steps, and most of the time independent from the magnitude of the measured physical quantity. In this lesson, we focus on this first step and we detail the methods allowing to determine the optical phase $\Delta\varphi$.

Optical phase demodulation methods have been employed since optical methods permit measuring of physical parameters, and that in a large diversity of application fields (mechanics, vibrations, thermics, fluid mechanics, work of art, materials...). For a long time, their use has been inhibited because the processing was done by hand. The phase quantification could be achieved only at extrema of the fringe pattern (i.e. at the points where the intensity reaches a minimum or a maximum), and the fringe pattern was simply photographed and overexposed to highlight these points. These processes were tedious and inefficient because it was very difficult to distinguish the signal from the noise.

During the 60s, the first video cameras and computers allowed acquiring and storing fringe patterns in a format suited for post-processing. The rapidity and performance of the measurement improved because new tools (such as statistical averages) became available to increase the contrast and decrease the noise, so that the extrema of the fringe patterns became easier to extract. Theses elementary methods were substituted in the middle of the 70s [1 [[01]],2 [[02]]] by the first techniques based on image processing which gave a direct access to the phase. The increase in computer speed and data storage combined with the decrease of their price facilitated their use and fast development. Today, these methods represent a versatile tool in optical metrology.

There are various methods allowing phase determination. Each of them has some specific advantages making them suitable for specific applications, but none of them is universal or optimal. One of the most widely used method is the phase shifting technique, for which the optical phase $\Delta\varphi$ is estimated using a sequence of phase-shifted fringe patterns, combined with an arctan function. Considering the importance of this method, we will explain it with

great details and we will also give a possible classification of various strategies for phase demodulation and error analysis.

1. Principle of phase demodulation

In general, phase demodulation methods make use of an optical phase modulation for which a additional phase term $\zeta(x,y,t)$ is added to the useful phase $\Delta\varphi$. The fringe pattern expression can thus be rewritten as:

$$I(x,y,z,t)=a(x,y,z,t)+\sum_{n=1}^{\infty} b_n(x,y,z,t)\cos\left(n\Delta\varphi(x,y,z,t)+n\zeta(x,y,t)\right)$$

This phase modulation can be purely temporal; in this case, it will produce a uniform phase shift in the plane of the fringe pattern:

$$\zeta(x,y,t)=2\pi f_0 t$$

The modulation can also be purely spatial:

$$\zeta(x,y,t)=2\pi u_0 x+2\pi v_0 y$$

In this latter case, the modulation introduces a phase variation in the image plane which is called "spatial carrier".

The parameters $u_0, v_0, 0$ are the carrier frequencies of the modulation. To describe the demodulation process, it is judicious to focus on the parameters of the carrier frequencies, since the terms $a(x,y,z,t)$ and $b_n(x,y,z,t)$ are generally independent from the modulation terms. A generic process of demodulation must then determine the phase $\Delta\varphi(x,y,z,t)$ independently from $a(x,y,z,t)$ and $b_n(x,y,z,t)$. Combining various techniques of phase extraction with one of the two types of modulation leads to a large variety of methods, each of them having their own algorithm, applicability, and performance.

Most of these methods assume a sinusoidal profile, which implies that the decomposition contains only one harmonic, but most of them can be applied to other profiles with minor modifications.

1.1. Classification of phase demodulation techniques

A first classification is based on the distinction between global and local methods. A local method computes the optical phase at a single point by using the successive values of the signal at this point, or by using an ensemble of values in a group of neighboring points. A global method will give the optical phase at all the points where the fringe pattern was registered. There is therefore a major difference between the two approaches: for the local method, the values of a, b_n and $\Delta\varphi$ stay constant within each calculation cell, whereas for the global method for which the calculation cell encompasses the full fringe pattern, the phase $\Delta\varphi$ varies in the field, and its evaluation depends on the ability to suppress the variations of a, b_n by isolating their contributions.

Another classification can be based on the distinction between temporal and spatial methods. In the first case, the data used for phase determination are obtained at various time intervals, whereas in the second case all the data is acquired simultaneously.

In this lesson, we decided to classify the methods depending whether they involve a spatial carrier or not. Indeed, the methods based on a spatial carrier utilize the same spatial domain to represent the image (the pixels), contrary to the other methods for which each pixel is examined independently from the others and at different time points, necessitating the acquisition of several fringe patterns taken at various time points.

The limitations of the spatial carrier technique thus appear in the dynamic range, and therefore in the spatial variations of the phase that are tolerable for this method. These limitations are related to the spectral overlapping effects, and can be expressed as a fraction of the carrier frequency, for which the ultimate limitation is the pixel density compared with the fringe density. However, these methods require the acquisition of only one fringe pattern to estimate the phase and are therefore well adapted to dynamic phenomenons: they can be described as real time methods.

According to this criterion, the methods will be classified as follows :

- Phase demodulation without spatial carrier
  - temporal phase shifting
  - phase stepping
  - spatial phase shifting
- Phase demodulation with spatial carrier
  - Fourier transform demodulation
  - phase shifting with spatial carrier
  - spatial lock-in demodulation

Each of these methods will be presented later on.

1.2. Ambiguity on the phase sign

When extracting the phase $\Delta\varphi$ from an interferogram using an analytic inversion of the fringe pattern, we have to solve the problem of the phase sign, which appears because the cosine function is not bijective but is even and periodic. Indeed, a phase determined using a single fringe pattern remains undefined with respect to the sign and to an additive constant, that is, an integer multiple of 2π. Each phase demodulation method includes an inverse trigonometric function. Each inverse trigonometric function can be expressed using the arctangent function, for example as $\arccos(x) = \arctan(\sqrt{1-x^2}/x^2)$.

The arctangent function gives a result included in the interval $[-\pi/2, +\pi/2]$.

For most phase demodulation techniques, the argument of the arctangent function is a ratio for which the numerator characterizes the phase sine and the denominator the phase cosine. It is thus interesting to consider numerator and denominator independently to obtain a value in the interval $[-\pi, +\pi]$ by considering the sign of each quantity. The four possible situations as for the sign of the sine, cosine and tangent are indicated on figure 1.

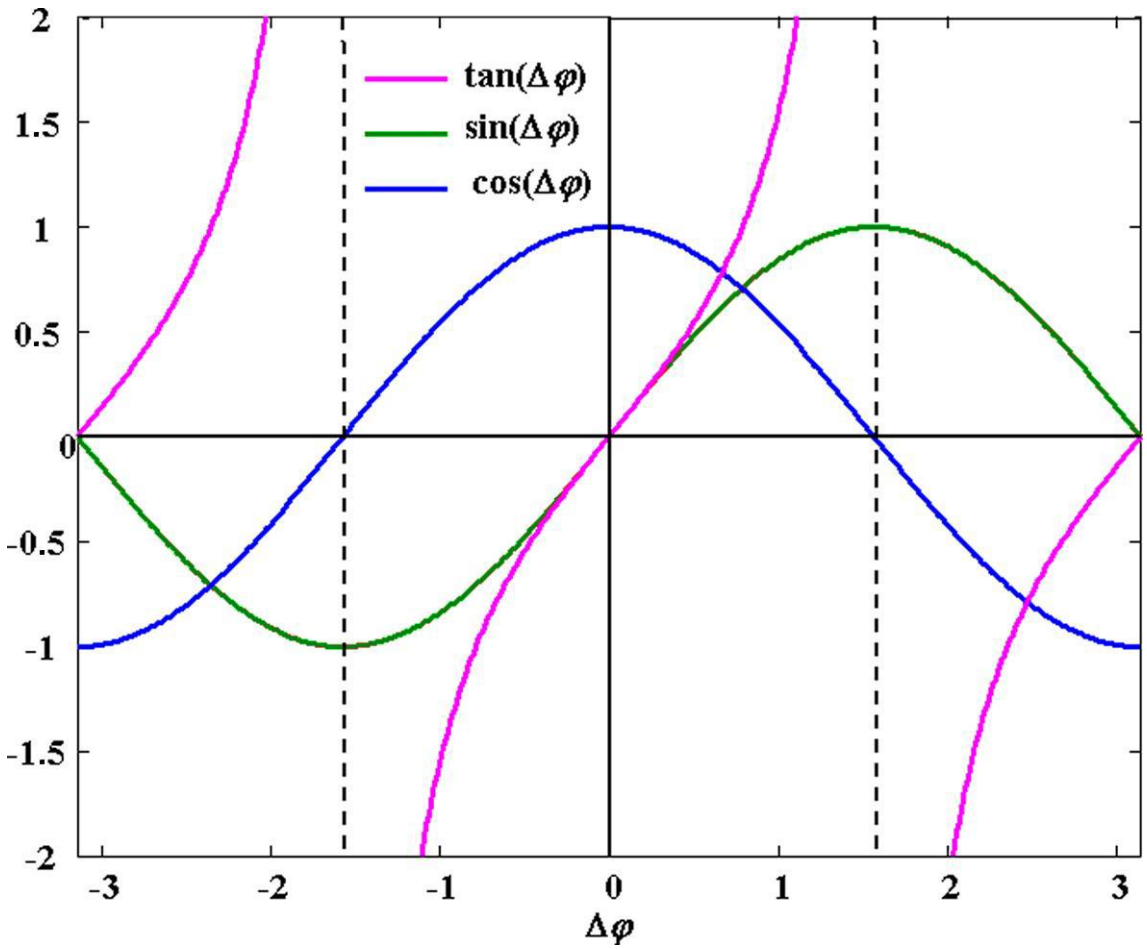

Figure 1 : signs of trigonometric functions

However, the previous step allows a determination on the interval $[-\pi, +\pi]$ and is not sufficient to suppress the ambiguity about the phase constant (i.e. modulo 2π) and the sign.

A convenient technique to extract the sign is to take into account some information about the experimental conditions generating the optical phase, and the signal distribution within the fringe pattern. For example, the direction in which the studied structure moves can be known *« a priori »*, which will determine the sign of the phase variation.

Remarque

To eliminate the ambiguity on the phase sign without using any *« a priori »* knowledge on the observed phenomenon, it will be necessary to introduce a spatial carrier or to register several fringe patterns with phase shifting for example.

1.3. Need for phase unwrapping

The 2π discontinuity of the extracted phase appears when an extreme value, $+\pi$ or $-\pi$, is reached; the phase then jumps to the other end of the interval, $-\pi$ or $+\pi$, even though physically the optical phase is continuous and relatively softly increasing or decreasing. As an example, let us consider a continuous phase proportional to a physical quantity (displacement, thickness, velocity...) varying linearly along a pixel row of the detector. This variation is illustrated on figure 2.

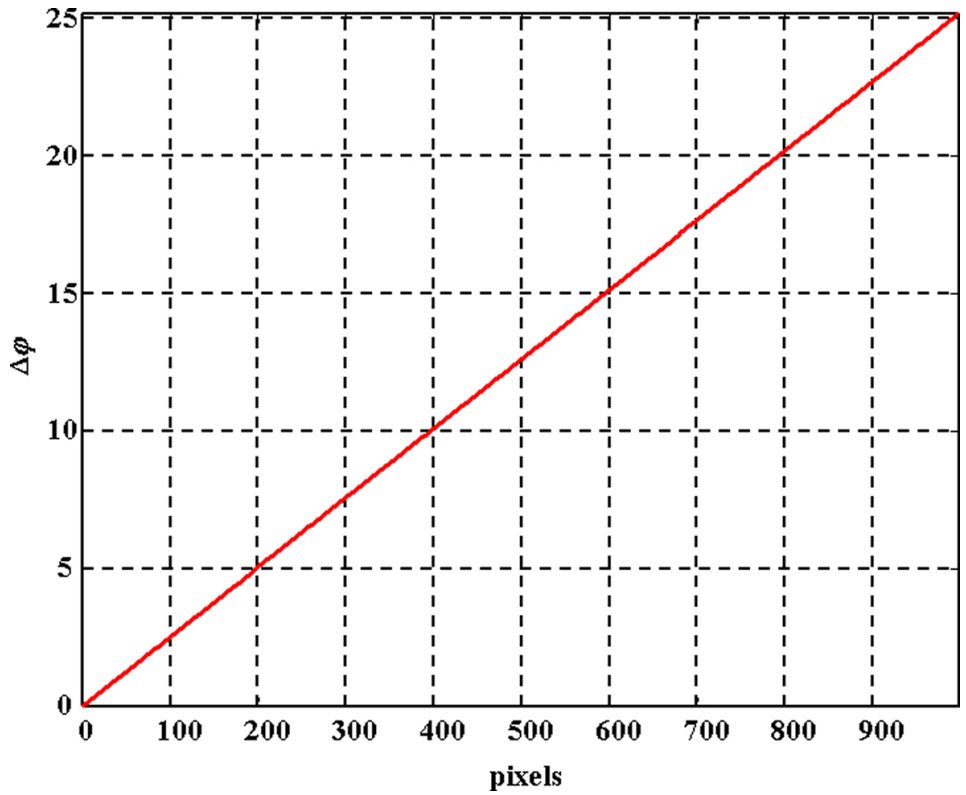

Figure 2 : continous variation of the optical phase

When demodulating the interferometric signal encoding for this variation, the arctangent function gives a wrapped phase variation, with phase jumps. This property is illustrated on figure 3.

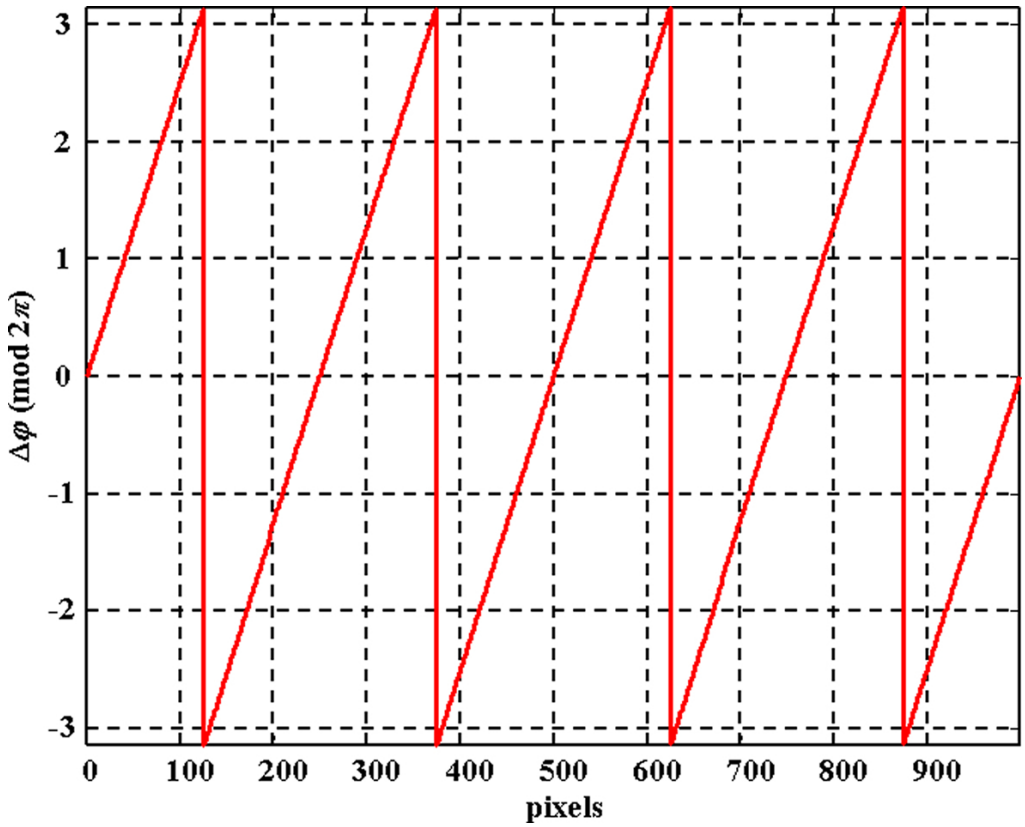

Figure 3 : discontinued variation of the optical phase

Reconstructing the physically continuous phase variation can be done by adding or subtracting multiples of 2π, and thereby suppressing the phase jumps. The operation consisting in determining the order of each fringe and therefore restoring the physical continuity of the phase map is called phase unwrapping [3 [[03]]]. The process usually begins at an arbitrary point of the phase map for which the order is equal to 0. After unwrapping, the phase can be considered to be known within an additional value. This value stays undetermined, unless it is possible to know a point in the phase map where the phase is indeed equal to zero. The problem vanishes for a light source of large spectrum (white light, for example), since the interference fringes are then located around a white fringe corresponding to a zero optical path difference.

Figure 4 represents a line of an experimental phase map obtained after demodulation. The phase jumps are clearly visible.

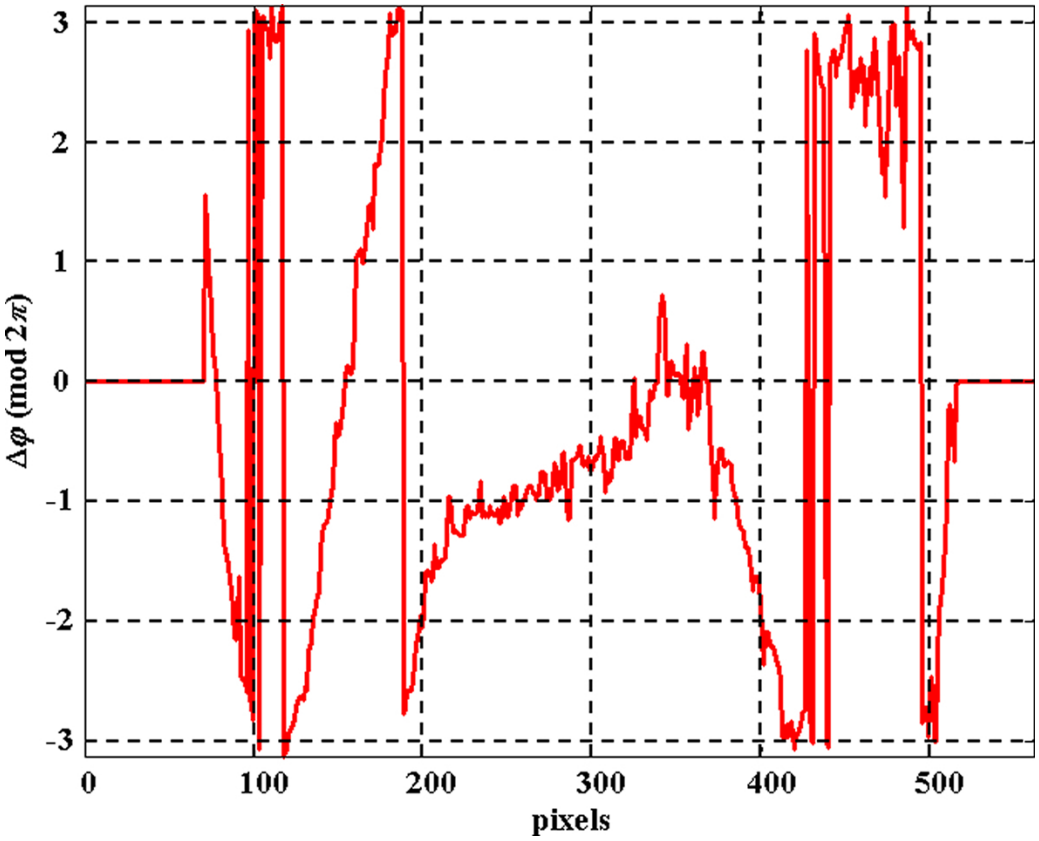

Figure 4 : wrapped phase (from an experiment)

Figure 5 shows the result obtained after unwrapping this phase. The starting point of the algorithm is located at pixel 300.

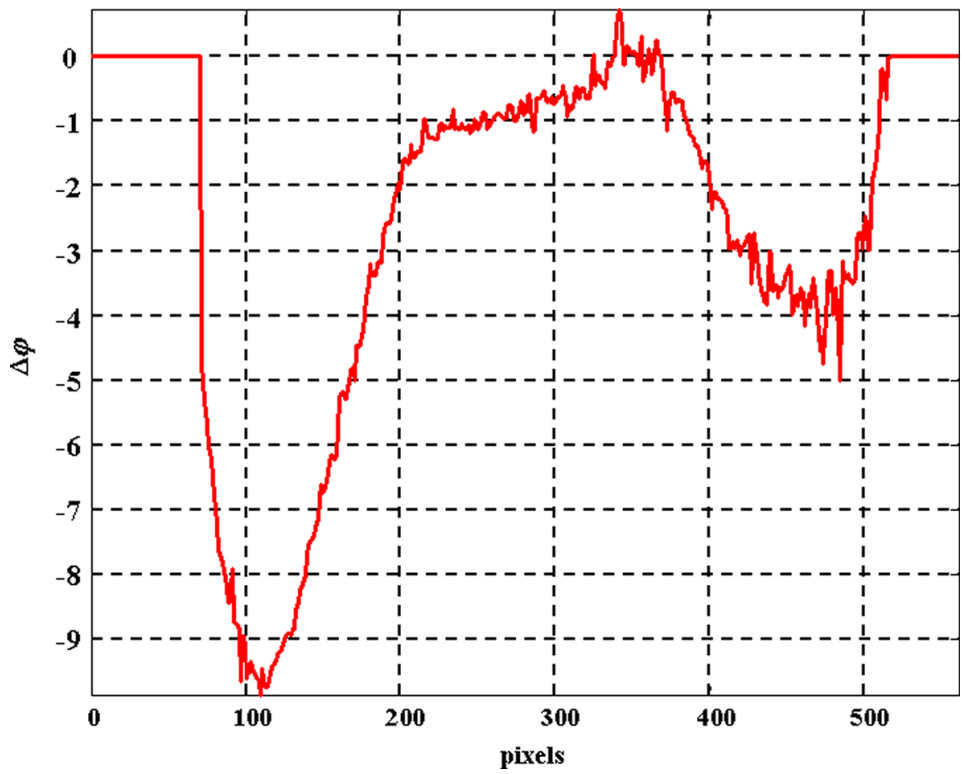

Figure 5 : unwrapped phase

The zero of this phase variation cannot be easily determined.

This result represents an introduction to phase unwrapping, and the various algorithms will not be detailed. Indeed, phase unwrapping techniques have become more and more sophisticated in the past 10 years with the appearance of powerful algorithms that are sometimes quite difficult to implement. For a complete description, the reader can use reference [3 [[03]]].

The unwrapping operation is relatively easy to implement when the number of pixels per fringe is large, and when the signal to noise ratio of the interferogram is high. In this case, unwrapping the phase consists in adding/subtracting $2\pi\ rad$ each time a discontinuity is detected in $\Delta\varphi$ modulo 2π. The phase map can be scanned vertically or horizontally. In practice, this ideal case is not very common because the noise level can be quite high, in particular for speckle interferometry methods. Phase unwrapping then becomes extremely complicated.

Remarque

In general, phase unwrapping algorithms must define a criteria to identify the discontinuities.

Algorithms can be classified into two categories:

- those independent from the path followed on the phase map, and called "**global**" algorithms; they operate in a single step by identifying, isolating and excluding the locations of $\Delta\varphi$ that could lead to an error when identifying discontinuities; the unwrapping process is done by following an arbitrary path on the phase map.
- those dependent on the followed path, which are called "**local**"algorithms; they give a continuous phase, point by point, by following a given path.

Recently developed phase unwrapping algorithms can be efficient even in the difficult situations where the noise level is comparable to the phase value, where interferograms show a small modulation, where the phase exhibits a steep phase jump due to a discontinuity of the measured physical value, or where the pixel density per fringe is small.

Algorithms will be distinguished according to their computation time, their sensitivity to error propagations during unwrapping, and their robustness to previously mentioned elements. Despite the large progress made in the past years, we have to mention that no algorithm can

behave positively when many sources of problems add up. Each of them is only efficient to solve one particular problem, and requires additional information to cover all cases. In that sense, up to now, no fully automated algorithm has been developed.

Exemple

For example, a possible strategy to make an algorithm insensitive to the noise of the phase map consists in comparing the point currently addressed with other points nearby for which the phase has already been unwrapped. To be insensitive to noise peaks, the comparison can be done after low-pass filtering the considered neighbourhood (using a mean or a median filter for example). Then, we consider the next point and use the same (or a slightly modified) neighborhood, and so on. The algorithm is thus propagated to the full image. To start unwrapping, the algorithm therefore requires the knowledge of a region where there is no phase jump. This region can be arbitrarily chosen in the image, or can be chosen by the experimentalist, who can identify a region where the fringe patterns density is small.

This strategy is therefore mostly insensitive to noise, but on the other hand is very sensitive to fringe openings (loss of continuity of the contour lines $\pm\pi$) and will propagate errors on the whole phase map. Nevertheless, the experimentalist will always have the possibility to work again on the problematic regions to improve the accuracy of the algorithm.

2. Phase demodulation without spatial carrier

2.1. Temporal phase shifting

This method requires a linear and uniform phase modulation over the field of view during the exposure time of the detector. This imposes:

$$\zeta(x,y,t)=2\pi f_0 t$$

A sequence of fringe patterns with a phase increment is registered and the phase difference covered during the exposure time must be identical from one acquisition to the next [1 [[01]],4 [[04]]]. If the optical phase is varying very rapidly with time, the acquisition must be done with a very high temporal bandwidth and in this case we are confronted with a technology problem, as the camera speed is rarely above 1000 images/s with a spatial resolution of 1024×1024 pixels. In the case where the phase is static (motionless) or quasi-static, the applied linear modulation can be "slow", and therefore the bandwidth can be lower, meaning that we register one image per camera cycle, typically 25 images/s. The detector temporally averages the fringes signal.

Let us consider the following sinusoidal phase profile:

$$I(t)=a+b\cos(\Delta\varphi+2\pi f_0 t)$$

The mean level (a) and contrast (b) are time independent. The spatial dependencies have been implied. $\Delta\varphi$ is the phase we want to determine (and is also time independent). Each image is obtained by integrating over a time interval ΔT :

$$E_n=\frac{1}{\Delta T}\int_{(n-1)\Delta T}^{n\Delta T} I(t)\,dt=a+\frac{b}{\Delta T}\int_{(n-1)\Delta T}^{n\Delta T}\cos(\Delta\varphi+2\pi f_0 t)\,dt$$

This technique is known as "**integrating bucket**". Figure 6 illustrates the acquisition process by showing the interferometric signal and the area under the curve which corresponds to the temporal integration over each time interval of duration ΔT.

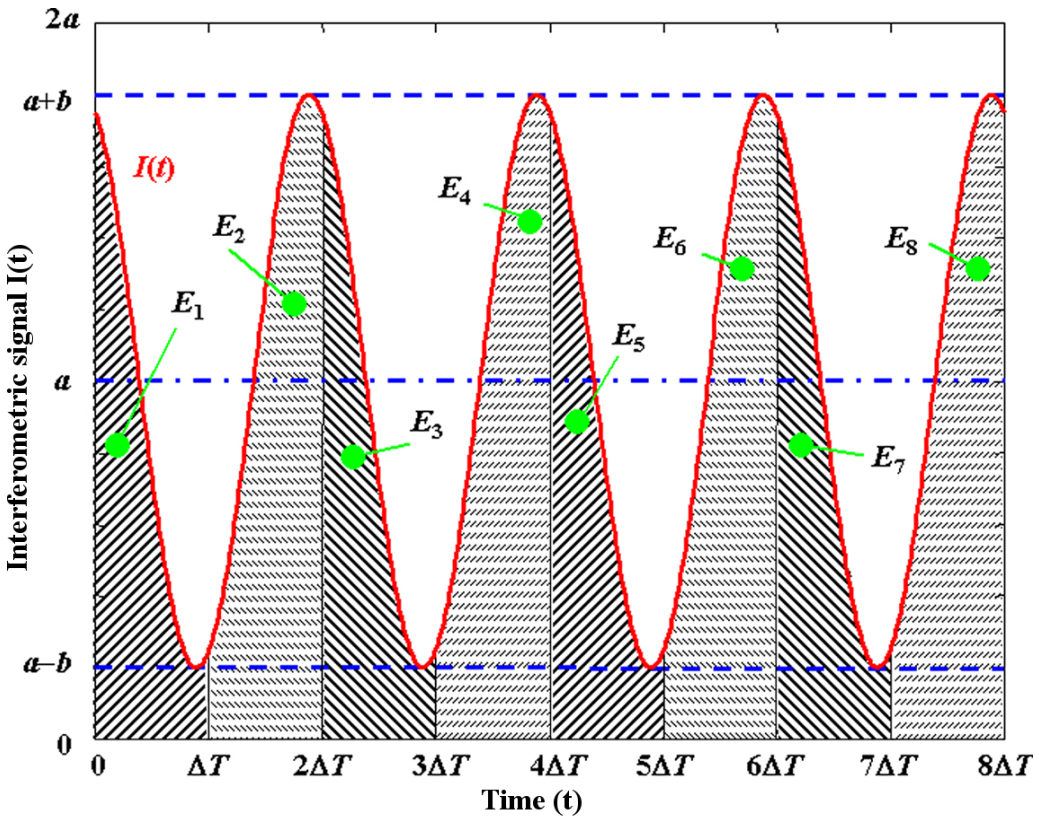

Figure 6 : interferometric signal and temporal integration

The calculation of the temporal integration yields:

$$E_n = a + b\ \mathrm{sinc}(\pi f_0 \Delta T)\cos(\Delta\varphi + 2\pi f_0 (n - \frac{1}{2})\Delta T)$$

We note $\phi = 2\pi f_0 \Delta t$, ϕ is the phase increment between each image. We then obtain:

$$E_n = a + b\ \mathrm{sinc}(\frac{\phi}{2})\cos(\Delta\varphi + n\phi - \frac{\phi}{2})$$

The values registered during each integration time are represented on figure 7. The samples follow a sine wave (dashed line) of smaller modulation than the initial signal.

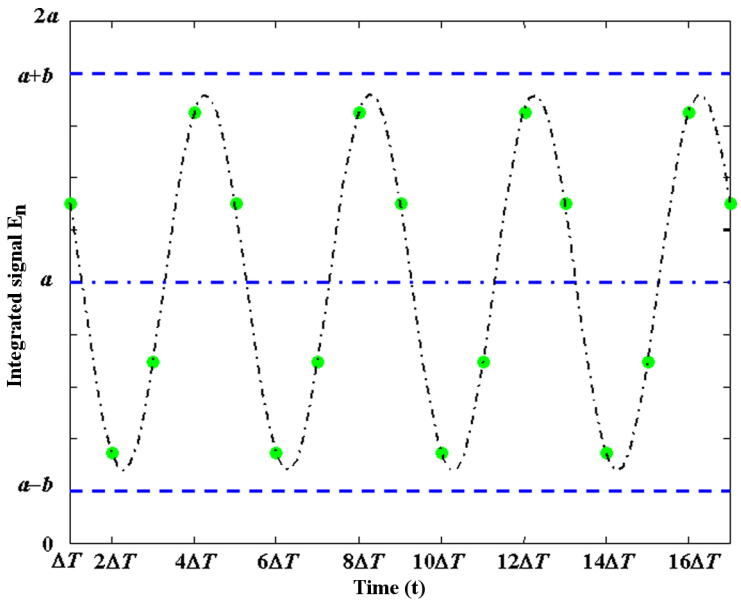

Figure 7 : samples of integrated signal

On a mathematical point of view, the expression of the temporally integrated interference signal has three unknowns $a, b, \Delta\varphi$, among which $\Delta\varphi$ is the main unknown to determine. To solve this problem, we therefore need at least three equations, thus generating a system of at least three equations with three unknowns. Solving this system will give the three parameters. If we register at least three interferograms E_n, then we will be able to determinate $\Delta\varphi$.

Remarque

This phase stepping method therefore consists in a tridimensional sampling of the fringe pattern: two planar dimensions with the coordinates on the image and one longitudinal dimension with the optical phase variation $\phi = 2\pi f_0 \Delta t$. The choice of ϕmust be done according to Shannon theorem, which tells us that we need to register at least two values of the signal per fringe period, thus imposing $\phi < \pi$.

Let us consider for example the case where ϕ is equal to $\pi/2$. Using a 25 Hz acquisition system, we have $\Delta t = 40$ ms and we will need to impose $_0 = 6.2$ Hz ; registering the 4 interferograms will give:

$$E_1 = a + b\ \mathrm{sinc}\left(\frac{\pi}{4}\right)\cos\left(\Delta\varphi - \frac{\pi}{4}\right)$$

$$E_2 = a + b\ \mathrm{sinc}\left(\frac{\pi}{4}\right)\cos\left(\Delta\varphi - \frac{\pi}{4} + \frac{\pi}{2}\right)$$

$$E_3 = a + b\ \mathrm{sinc}\left(\frac{\pi}{4}\right)\cos\left(\Delta\varphi - \frac{\pi}{4} + \pi\right)$$

$$E_4 = a + b\ \mathrm{sinc}\left(\frac{\pi}{4}\right)\cos\left(\Delta\varphi - \frac{\pi}{4} + \frac{3\pi}{2}\right)$$

Fringe modulation is reduced by approximately 10% since $sinc(\pi/4) = 0.9$. We obtain $\Delta\varphi$ using an $arctangent$ function:

$$\Delta\varphi = \arctan\left(\frac{E_4 - E_2}{E_1 - E_3}\right) + \frac{\pi}{4}$$

The amplitude of fringe oscillation is:

$$b|\mathrm{sinc}(\pi/4)| = \frac{1}{2}\sqrt{(E_1 - E_3)^2 + (E_4 - E_2)^2}$$

and the constant component of the signal is given by:

$$a = \frac{1}{4}(E_1 + E_2 + E_3 + E_4)$$

We can thus determine the modulation ratio of the fringe pattern:

$$m = \frac{b|\mathrm{sinc}(\pi/4)|}{a} = \frac{2\sqrt{(E_1 - E_3)^2 + (E_4 - E_2)^2}}{E_1 + E_2 + E_3 + E_4}$$

The determination of this modulation ratio can be used to extract the useful region for processing interferograms. Indeed, only pixels for which the modulation is above a certain threshold (for example $\mathrm{m} > 10\%$) should be processed and therefore they will be affected a value of 1 in the image mask, whereas the other pixels ($\mathrm{m} < 10\%$) will be affected to a value of 0 in the mask. The analysing software will process only pixels for which the mask value is 1.

2.2. Phase stepping

In this case, the phase modulation is a step that we maintain constant during the integration time of the detector [2 [[02]],4 [[04]]]. We are not imposing a phase ramp as in the previous case but successive phase steps. The instantaneous signal therefore reads:

$$I(t) = a + b\cos(\Delta\varphi + 2\pi\phi(t))$$

and the signal integrated by the detector during the time interval Δt, during which $\phi(t)$is constant and equal to ϕ_n, can be written as:

$$E_n = a + b\cos(\Delta\varphi + \phi_n)$$

Phase stepping is illustrated on figure 8.

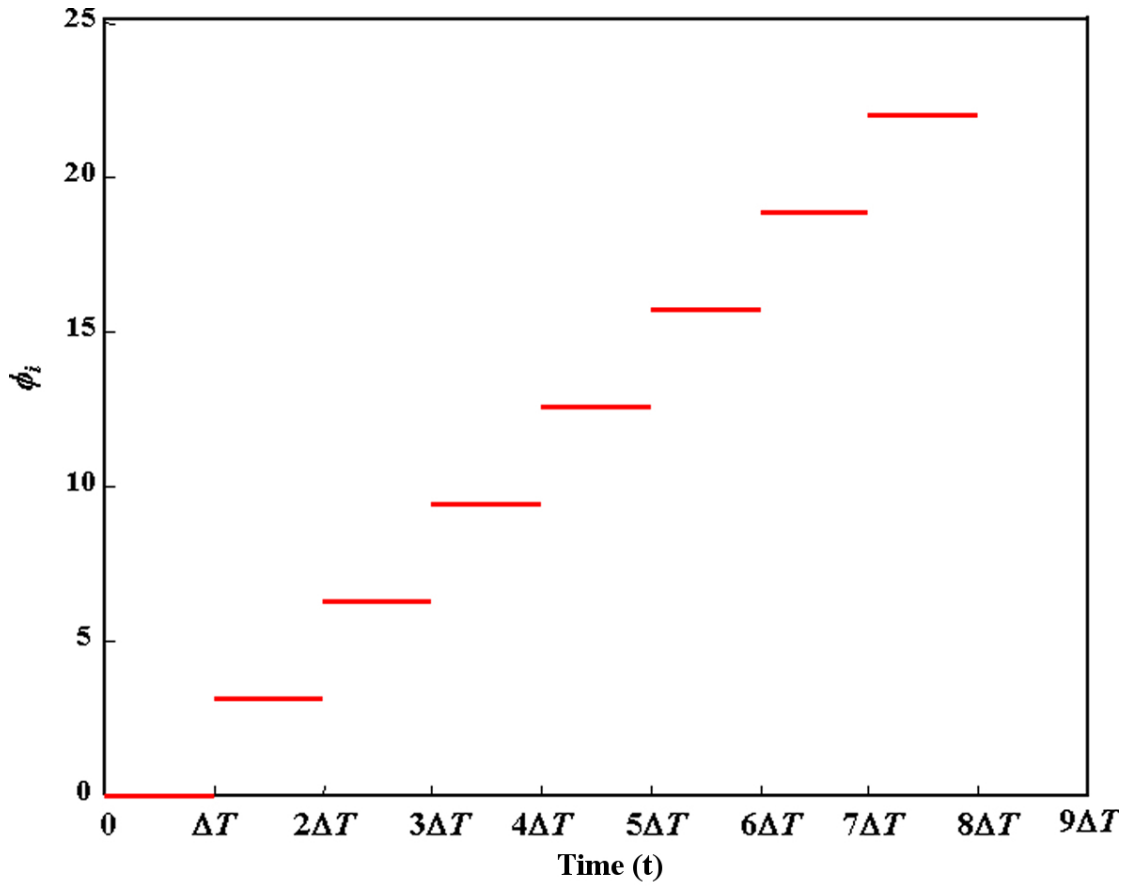

Figure 8 : phase stepping

The values registered for each phase step are represented on figure 9. The samples follow a sine wave (represented with a dotted line) with the same modulation and phase.

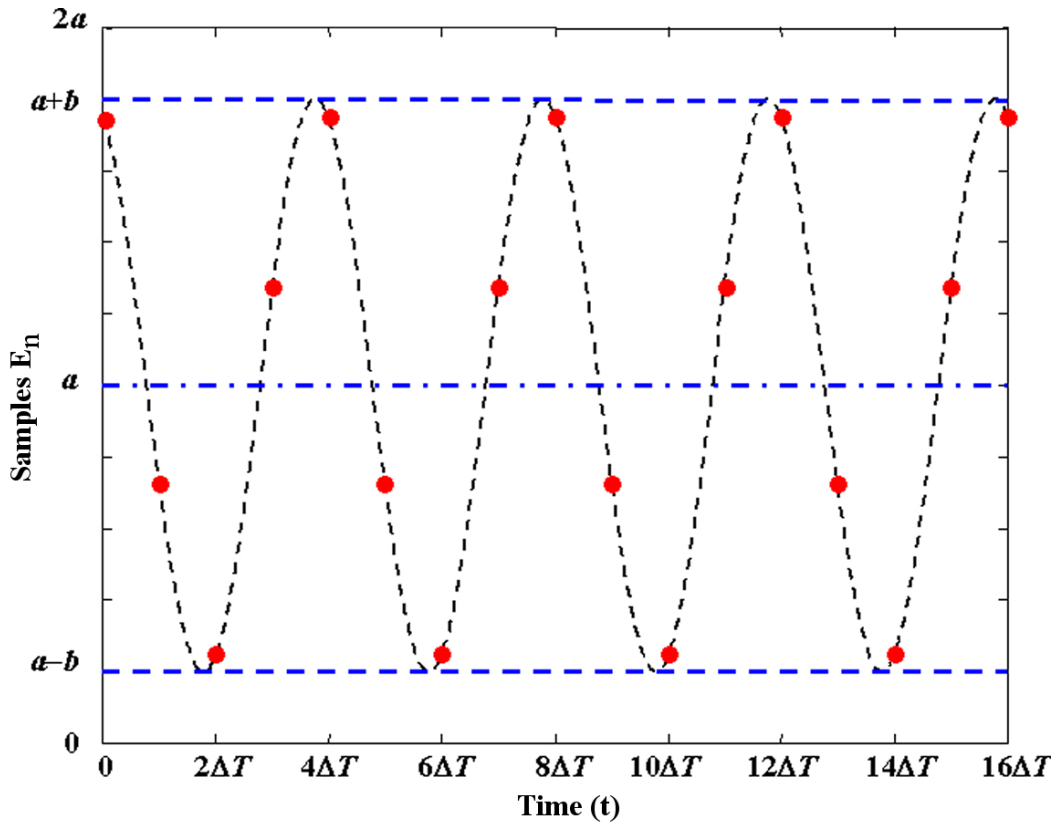

Figure 9 : registered samples

We consider the case where three images are registered with $\phi_1 = 0$, $\phi_2 = 2\pi/3$ and $\phi_3 = 4\pi/3$; we obtain the following equation system:

$$E_1 = a + b\cos(\Delta\varphi)$$
$$E_2 = a + b\cos(\Delta\varphi + 2\pi/3)$$
$$E_3 = a + b\cos(\Delta\varphi + 4\pi/3)$$

By developing the cosine functions, we obtain :

$$E_2 = a - \frac{1}{2}b\cos(\Delta\varphi) - \frac{\sqrt{3}}{2}b\sin(\Delta\varphi)$$
$$E_3 = a - \frac{1}{2}b\cos(\Delta\varphi) + \frac{\sqrt{3}}{2}b\sin(\Delta\varphi)$$

and since:

$$2E_1 - E_2 - E_3 = 3b\cos(\Delta\varphi)$$
$$E_3 - E_2 = \sqrt{3}b\sin(\Delta\varphi)$$

we obtain $\Delta\varphi$ the phase using an arctangent function:

$$\Delta\varphi = \arctan\left(\frac{3}{\sqrt{3}}\frac{E_3 - E_2}{2E_1 - E_2 - E_3}\right)$$

The amplitude of fringes oscillation can be evaluated by:

$$b=\frac{1}{\sqrt{3}}\sqrt{\frac{1}{3}(2E_1-E_2-E_3)^2+(E_3-E_2)^2}$$

and the constant component of the signal reads:

$$a=\frac{1}{3}(E_1+E_2+E_3)$$

Therefore, we can determine the modulation ratio of the fringe pattern:

$$m=\sqrt{3}\,\frac{\sqrt{\frac{1}{3}(2E_1-E_2-E_3)^2+(E_3-E_2)^2}}{E_1+E_2+E_3}$$

This technique is known as "**phase stepping**".

2.3. Generalization

The phase shifting method was first introduced in 1966 [5 [[05]]], when P. Carré invented this processing method for the interferential comparator of the BIPM (International Office for Weights and Measurements).

Remarque

This technique has the advantage that it doesn't require any intervention from an experimentalist after the interferograms have been registered. This is actually the reason why this method is widely used in some commercially available devices: Fizeau interferometer, interferential microscope, fringe pattern projection, shearography, etc. Phase shifting algorithms usually assume that the fringe pattern has a sinusoidal profile characteristic of two-wave interferences. The interferogram can thus be written, in a general way:

$$E_n=a+b\cos(\Delta\varphi+(n-1)\phi)\quad n=1,2,3,\ldots,N$$

where ϕ is "**the phase shift** ", and where the spatial and possibly temporal dependencies have been implied. Using this simple expression, which contains three unknowns, a, b, $\Delta\phi$, or possibly four with ϕ depending on the degree of knowledge of ϕ , one needs at least three equations to determine all variables. Thus, if ϕ takes successively N values, one will obtain a system of N equations with three (or four) variables which can be solved.

The **main advantages of phase shifting** are the follwing:

- a small sensitivity to stationary noise in the range on which ϕ varies; for example, for temporal phase shifting the algorithm is insensitive to the nonuniformity of a and b and to the variation of detector sensitivity from one pixel to another.
- the algorithms can be used with poorly contrasted fringe patterns.
- the uncertainty on the result is limited by the signal to noise ratio of the fringe pattern; systematic errors can be sufficiently reduced so that the noise will be the factor limiting the uncertainty.
- the analysis process of the fringe pattern can be fully automated.
- the optical phase $\Delta\varphi$ is determined at each point of the interferogram.
- spatial resolution is high since the number of points for which the phase is measured coincides with the number of pixels of the acquisition sensor.

- the high computation power available today (PC included) enables calculation of times smaller than $1\ s$.

In fact, the main limitation of these algorithms is that the phase is calculated modulo 2π. Moreover, the smallest fringe period in the camera acquisition plane must be larger than $2\ pixels$.

Phase shifting algorithms can be classified using several criteria. We will use a classification in two groups: the larger group will bring together the algorithms that we will call "**generic**", obtained by a systematic processing. The second group will contain the so-called "**specific** " algorithms, for which the previous hypothesis are non valid and $\Delta\varphi$ cannot be the result of direct systematic processing [6 [[06]]].

For this lesson, we will focus on generic algorithms.

2.4. Generic algorithms

This algorithms use known values of the phase shift ϕ, which means that only three unknown of the interference equation remain to be determined: $a,\ b,\ \Delta\varphi$. Therefore, only three interferograms are needed in order to solve the problem. A generic formulation of an algorithm with *N* interferograms can be obtained considering the least square criteria. Greivenkamp [7 [[07]]] used this approach in 1984. The interferogram can be written:

$$E_n = a_0 + a_1\cos(\phi_n) + a_2\sin(\phi_n) \quad n \in [1,2,3,\ldots,N]$$

The unknown are now: $a_0 = a, a_1 = b\cos(\Delta\varphi)$ and $a_2 = b\sin(\Delta\varphi)$. In the least square sense, the interferograms must minimise the following criterion:

$$\varepsilon = \sum_{n=1}^{N}\left[E_n - (a_0 + a_1\cos(\phi_n) + a_2\sin(\phi_n))\right]^2$$

ϵ is minimum when the partial derivatives with respect to the three parameters are equal to zero:

$$\frac{\partial\varepsilon}{\partial a_0} = \frac{\partial\varepsilon}{\partial a_1} = \frac{\partial\varepsilon}{\partial a_2} = 0$$

This leads to a linear system of three equations with three unknowns. We have:

$$\begin{aligned}
&\sum_{n=1}^{n=N} a_0 + a_1\cos(\phi_n) + a_2\sin(\phi_n) = \sum_{n=1}^{n=N} E_n \\
&\sum_{n=1}^{n=N} a_0\cos(\phi_n) + a_1\cos^2(\phi_n) + a_2\cos(\phi_n)\sin(\phi_n) = \sum_{n=1}^{n=N} E_n\cos(\phi_n) \\
&\sum_{n=1}^{n=N} a_0\sin(\phi_n) + a_1\cos(\phi_n)\sin(\phi_n) + a_2\sin^2(\phi_n) = \sum_{n=1}^{n=N} E_n\sin(\phi_n)
\end{aligned}$$

which can also be written as:

$$A(\phi_n)\,X = B(E_n, \phi_n)$$

with

$$A(\phi_n)=\begin{pmatrix} N & \sum_{n=1}^{n=N}\cos(\phi_n) & \sum_{n=1}^{n=N}\sin(\phi_n) \\ \sum_{n=1}^{n=N}\cos(\phi_n) & \sum_{n=1}^{n=N}\cos^2(\phi_n) & \sum_{n=1}^{n=N}\cos(\phi_n)\sin(\phi_n) \\ \sum_{n=1}^{n=N}\sin(\phi_n) & \sum_{n=1}^{n=N}\cos(\phi_n)\sin(\phi_n) & \sum_{n=1}^{n=N}\sin^2(\phi_n) \end{pmatrix}$$

$$X=\begin{pmatrix} a_0 \\ a_1 \\ b_1 \end{pmatrix}$$

$$B(E_n,\phi_n)=\begin{pmatrix} \sum_{n=1}^{n=N}E_n \\ \sum_{n=1}^{n=N}E_n\cos(\phi_n) \\ \sum_{n=1}^{n=N}E_n\sin(\phi_n) \end{pmatrix}$$

Inverting this equation gives:

$$X=A^{-1}(\phi_n)\,B(E_n,\phi_n)$$

Therefore, by inverting $A(\phi_n)$, we obtain a_0, $a_1$and $a_2$and the optical phase by:

$$\Delta\varphi=\arctan\left(\frac{a_2}{a_1}\right)$$

The amplitude of modulation at each point of the interferogram is

$$b=\sqrt{a_1^2+a_2^2}$$

If we judiciously choose the phase shift, the matrix $A(\phi_n)$ becomes diagonal. Indeed, if $\phi = 2\pi/N$ with $\phi_n = (n-1)\phi = 2(n-1)\pi/N$, the expression giving $\Delta\varphi$ becomes simple:

$$\Delta\varphi=\arctan\left(\frac{\sum_{n=1}^{n=N}E_n\sin((n-1)\phi)}{\sum_{n=1}^{n=N}E_n\cos((n-1)\phi)}\right)$$

With $N = 4$ and $\phi = \pi/2$, we recover the 4-images-algorithm previously described:

$$\Delta\varphi = \arctan\left(\frac{E_4 - E_2}{E_1 - E_3}\right)$$

and with $N = 3$ and $\phi = 2\pi/3$, we recover the 3-images-algorithm [6 [[06]],8 [[08]]] :

$$\Delta\varphi = \arctan\left(\frac{3}{\sqrt{3}}\frac{E_3 - E_2}{2E_1 - E_2 - E_3}\right)$$

However, the algorithms built according to this scheme do not always have an optimal behavior in the presence of error sources. This is why other approaches have been developed. Phase shifting algorithms robust to random errors can be conceived by using the maximum likelihood theory, or, for systematic errors, by using a combination of pre-existing algorithms.

For example, in 1983 J. Schwider [9 [[09]]] showed that an average value of the optical phase can be computed using a classical algorithm. The strategy relies on evaluating the phase with the $N-1$ first interferograms, and with the $N-1$ last interferograms, and to calculate the mean of the two results. If we consider $N = 4$ and $\phi = \pi/2$, we have one one hand

$$\Delta\varphi_1 = \arctan\left(\frac{2E_2 - E_1 - E_3}{E_3 - E_1}\right)$$

and on the other hand

$$\Delta\varphi_2 = \arctan\left(\frac{2E_3 - E_2 - E_4}{E_4 - E_2}\right) - \frac{\pi}{4}$$

and the average value is given by:

$$\Delta\varphi = \frac{1}{2}(\Delta\varphi_1 + \Delta\varphi_2)$$

This type of algorithm is less sensitive to calibration errors of the element producing the phase shift.

Complément

We have seen, in a non-exhaustive way, that there are a large number of algorithms available in the literature. Before choosing one of them, the user must therefore establish the requirements in terms of performance of the phase determination, as well as a list of the major sources limiting the precision. He will then have to choose the best compromise between **sensitivity/rapidity/simplicity**.

2.5. Sinusoidal phase modulation

In this technique, the phase is modulated by a sine wave in the frequency range of $10\ Hz$ to several hundreds of Hz [10 [[10]]]. The phase modulation therefore reads:

$$\zeta(x, y, t) = 2\pi f_0 \sin(\omega t + \varphi)$$

where $\omega = 2\pi$ is the frequency of the phase modulation, φ its synchronisation phase, and $2\pi f_0$ its amplitude. We still consider a sinusoidal phase profile, of constant amplitude, contrast, and phase offset. The spatial dependency being implied, we have:

$$I(t)=a+b\cos(\Delta\varphi+2\pi f_0\sin(\omega t+\varphi))$$

The signal is integrated successively during 4 quarters of the modulation period $\Delta t = 2\pi/\omega$, therefore:

$$E_n=\frac{4}{\Delta T}\int_{(n-1)\Delta T/4}^{n\Delta T/4} I(t)\,dt$$

We develop $I(t)$ in series of Bessel functions of the first kind:

$$I(t)=a+b\cos(\Delta\varphi)J_0(2\pi f_0)+2b\cos(\Delta\varphi)\sum_{n=1}^{\infty}J_{2n}(2\pi f_0)\cos(2n\omega t+2n\varphi)$$
$$-2b\sin(\Delta\varphi)\sum_{n=0}^{\infty}J_{2n+1}(2\pi f_0)\sin((2n+1)\omega t+(2n+1)\varphi)$$

We can write the result of the temporal integration as:

$$E_n=a+b\,A_n\cos(\Delta\varphi)+b\,B_n\sin(\Delta\varphi)$$

with:

$$A_n=J_0(2\pi f_0)+\frac{4}{\pi}\sum_{k=1}^{\infty}\frac{J_{2k}(2\pi f_0)}{2k}(\sin(kn\pi+2k\varphi)-\sin(k(n-1)\pi+2k\varphi))$$

$$B_n=-\frac{4}{\pi}-\sum_{k=1}^{\infty}\frac{J_{2k+1}(2\pi f_0)}{2k+1}\cos((2k+1)n\pi/2+(2k+1)\varphi)$$
$$+\sum_{k=1}^{\infty}\frac{J_{2k+1}(2\pi f_0)}{2k+1}\cos((2k+1)(n-1)\pi/2+(2k+1)\varphi)$$

and for each interferogram:

$$A_1=A_3=J_0(2\pi f_0)+\frac{4}{\pi}\sum_{k=1}^{\infty}\frac{J_{2k}(2\pi f_0)}{2k}(1-(-1)^k)\sin(2k\varphi)$$

$$A_2=A_4=J_0(2\pi f_0)-\frac{4}{\pi}\sum_{k=1}^{\infty}\frac{J_{2k}(2\pi f_0)}{2k}(1-(-1)^k)\sin(2k\varphi)$$

$$B_1=-B_3=\frac{-4}{\pi}\sum_{k=1}^{\infty}\frac{J_{2k+1}(2\pi f_0)}{2k+1}((-1)^k\sin((2k+1)\varphi)+\cos((2k+1)\varphi))$$

$$B_2 = -B_4 = \frac{-4}{\pi} \sum_{k=1}^{\infty} \frac{J_{2k+1}(2\pi f_0)}{2k+1} ((-1)^k \sin((2k+1)\varphi) - \cos((2k+1)\varphi))$$

which gives the following system:

$$\begin{aligned} E_1 &= a + b\, A_1 \cos(\Delta\varphi) + b\, B_1 \sin(\Delta\varphi) \\ E_2 &= a + b\, A_2 \cos(\Delta\varphi) + b\, B_2 \sin(\Delta\varphi) \\ E_3 &= a + b\, A_1 \cos(\Delta\varphi) - b\, B_1 \sin(\Delta\varphi) \\ E_4 &= a + b\, A_2 \cos(\Delta\varphi) - b\, B_2 \sin(\Delta\varphi) \end{aligned}$$

from which we deduce:

$$\begin{aligned} b\cos(\Delta\varphi) &= \frac{E_1 - E_2 + E_3 - E_4}{2(A_1 - A_2)} \\ b\sin(\Delta\varphi) &= \frac{E_1 + E_2 - E_3 - E_4}{2(B_1 + B_2)} \end{aligned}$$

and the phase is obtained by a arctangent function:

$$\Delta\varphi = \arctan\left(\alpha \frac{E_1 + E_2 - E_3 - E_4}{E_1 - E_2 + E_3 - E_4}\right) \qquad \alpha = \frac{A_1 - A_2}{B_1 + B_2}$$

α can be calculated using the equations:

$$A_1 - A_2 = \frac{8}{\pi} \sum_{k=0}^{\infty} \frac{J_{4k+2}(2\pi f_0)}{4k+2} \sin((4k+2)\varphi)$$

$$B_1 + B_2 = \frac{-8}{\pi} \sum_{k=0}^{\infty} (-1)^k \frac{J_{2k+1}(2\pi f_0)}{2k+1} \sin((2k+1)\varphi)$$

A study of the algorithm taking into account an additive noise on the integrated intensity shows that the noise influence is minimum for $2\pi f_0 = 2.45$ rad and $\varphi = 0.977$ rad[10 [[10]]]. For example, for a real time acquisition with a camera giving 200 images/s over a matrix of 256×256 pixels, the modulation frequency must be of 50 Hz to register a quarter of period in 2 ms.

Remarque

This method requires more complex calculations than the two previous methods but allows measuring the phase with a very high precision. Moreover, it is insensitive to various perturbations such as thermal fluctuation or mechanical variations of small frequency compared with the modulation frequency.

2.6. Phase shifting techniques

Phase shifting can be obtained with various optical elements. The most widely used techniques are:

- piezoelectric transducers

- electro-optic modulators
- acousto-optic modulators

Phase shifting with a piezo-electric transducer cconsists in gluing a mirror to a transducer to which a voltage is applied. The voltage then distorts the piezoelectric and the mirror moves, producing a small variation of the optical phase. If the light beam is reflected at normal incidence, a displacement of $\lambda/8$ is enough to produce a phase shift of $\pi/2$.

This method is illustrated on figure 10. The voltages applied to the crystal are generally on the order of several tens of volts.

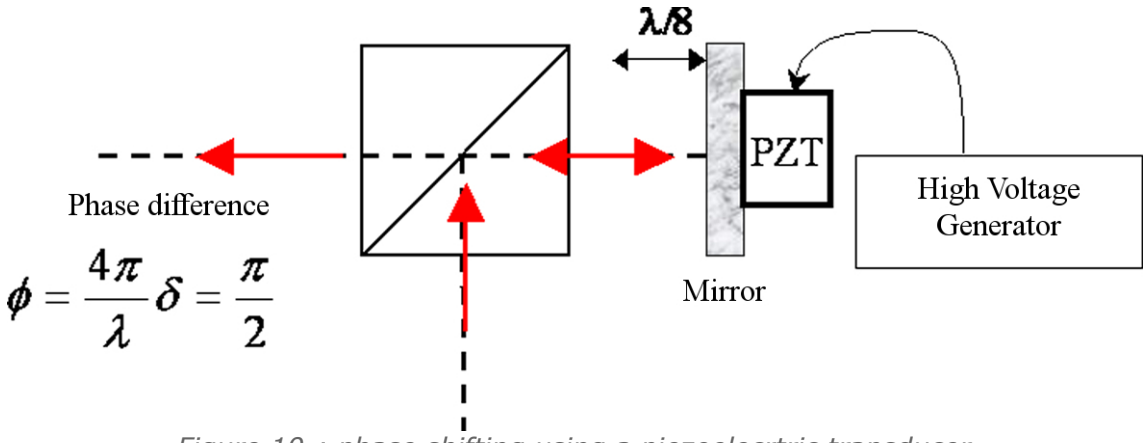

Figure 10 : phase shifting using a piezoelecrtric transducer

The piezoelectric crystal is generally driven with voltage steps. Driving the piezo with sinusoidal voltage is also possible if modulation frequencies too close to the resonance frequencies are avoided (since they could severely damage the crystal). This technique is probably the most widely used technique in commercially available interferometers. However, it is very sensitive to environment perturbations such as transverse vibrations. Indeed, such perturbations induce vibrations into the crystal and the mirror, thus altering the phase shift between interferograms.

Phase shifting with an electro-optic modulator makes use of light polarization. Consequently, it requires an interferometer working with polarized beams. The modulator is placed in the interferometer before the beams are separated, and the polarization of the incident wave is oriented at 45 from the neutral axes of the modulator. By applying a high voltage to the crystal, a birefringence is induced in the material, which in turns induces a phase difference between the two polarizations propagating in the medium. For example with a lithium niobate crystal ($LiNbO_3$) in transverse configuration, the phase difference is given by the following relation:

$$\phi = \frac{\pi}{\lambda}\left(n_e^3 r_{33} - n_o^3 r_{13}\right) L \frac{V}{d}$$

where V is the applied voltage, L the crystal length, d its thickness, n_0, n_e the ordinary and extraordinary refractive indexes of the crystal, and r_{13} , $r_{33}$the coefficients of the electro-optic tensor:

$$|r| = \begin{pmatrix} 0 & -r_{22} & r_{13} \\ 0 & r_{22} & r_{13} \\ 0 & 0 & r_{33} \\ 0 & r_{51} & 0 \\ r_{51} & 0 & 0 \\ -r_{22} & 0 & 0 \end{pmatrix}$$

The values of these coefficients are : $r_{13} = 8.10 \times 10^{-12}$ m/V and $r_{33} = 30.4 \times 10^{-12}$ m/V. Generally, the sensitivities are on the order of $\phi = 1,5 \times V$ mrad for visible wavelengths. Figure 11 shows the modulator configuration. The incident beam is linearly polarized in the plane (OXZ).

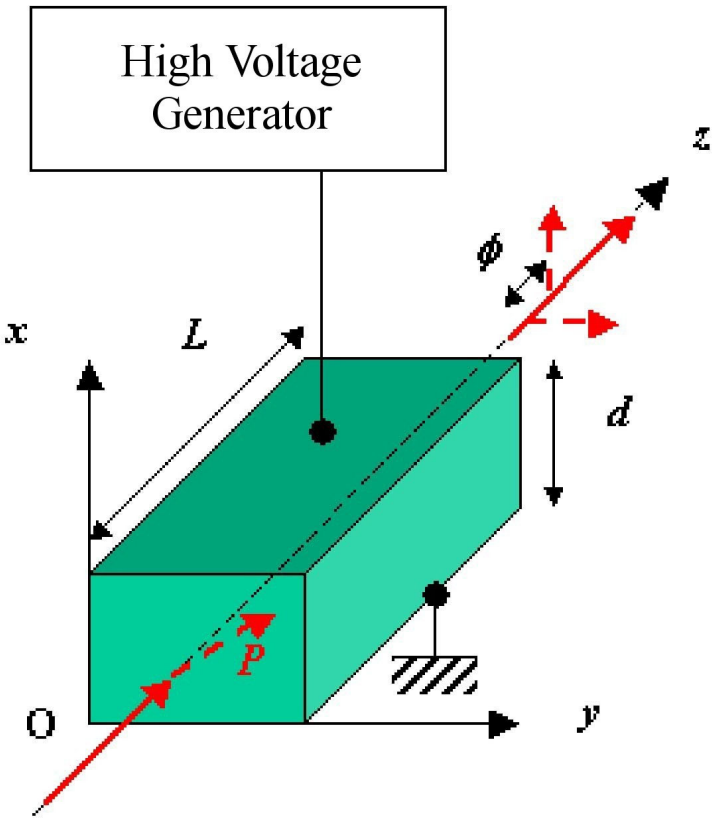

Figure 11 : LiNbO3 crystal in a transverse configuration

The crystal can be driven with voltage steps (for phase stepping), or with a sinusoidal voltage (for a sinusoidal modulation) with a frequency of several hundreds hertz.

In the case where an **acousto-optic crystal** (TeO_2, KRS_5, HgS) is used, the crystal generates an acoustic wave of wavelength λ_{ac} in the medium of optical index n (in the visible). The acoustic wave induces a variation of refractive index by photo-elastic effect. This index grating moves at the velocity of the acoustic wave but stays static in appearance for the optical wave which is thus diffracted. In the Bragg regime, when the acoustic wavelength is much smaller than the crystal thickness, and for an incident angle such that

$$\sin(\theta_B) = \frac{\lambda}{2 n \lambda_{ac}}$$

the light beam is diffracted into a single order and its frequency is shifted of a quantity equal to the acoustic wave frequency, f_{ac}. The modulator configuration is illustrated on figure 12.

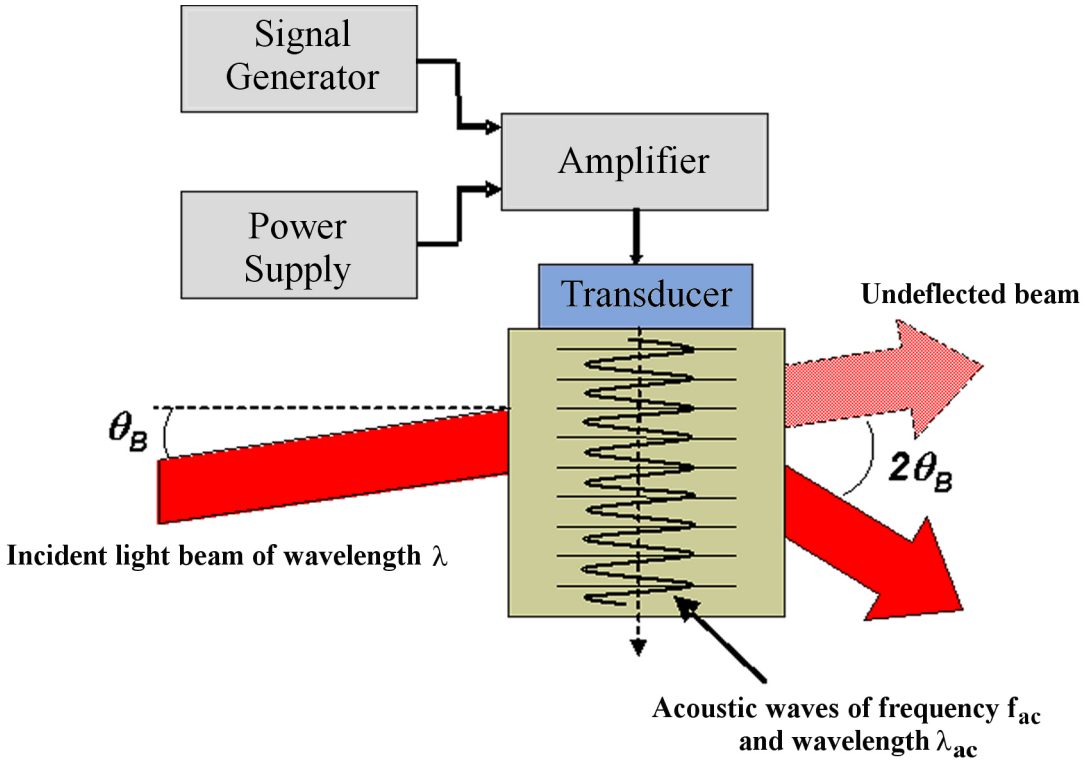

Figure 12 : acousto-optic diffraction

When the diffracted beam interferes with a non-diffracted beam, the resulting intensity contains a phase modulation term given by $2\pi f_{ac} t$. The technique of "**phase bucket**" can therefore be applied. The acoustic frequencies are generally ranging from a few Mhz to more than $100\ Mhz$ for some modulators.

Generally, 2 modulators are used, one on each beam with a small frequency difference of Δf_{ac} such that the phase modulation term is $2\pi\Delta f_{ac} t$ and becomes compatible with the usual frame rates of the sensors.

2.7. Illustrations

This paragraph presents an illustration of the phase stepping method. We consider an interferogram with a fringe pattern such as the one represented on figure 13.

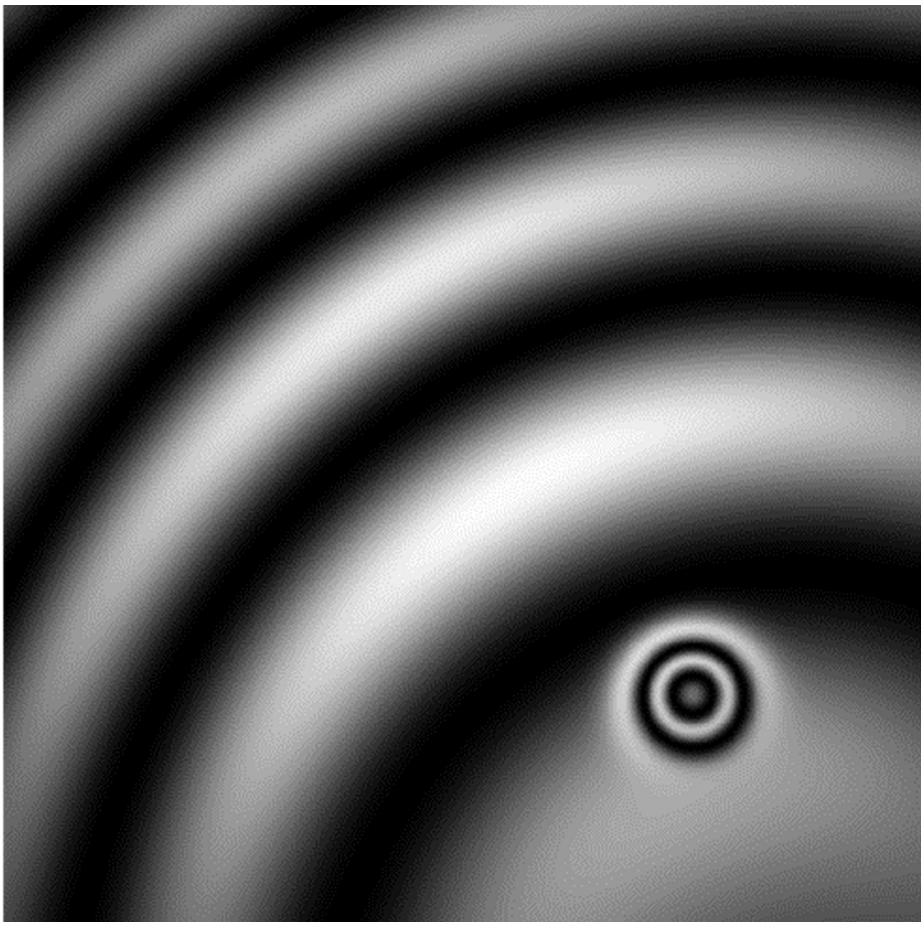

Figure 13 : instantaneous interferogram

We now apply the phase stepping method with 4 phase steps separated by $\pi/2$, generated (for example) with a piezoelectric transducer. Figure 14 shows the 4 shifted interferograms, obtained with phase steps of 0, $\pi/2$, π and $3\pi/2$ respectively.

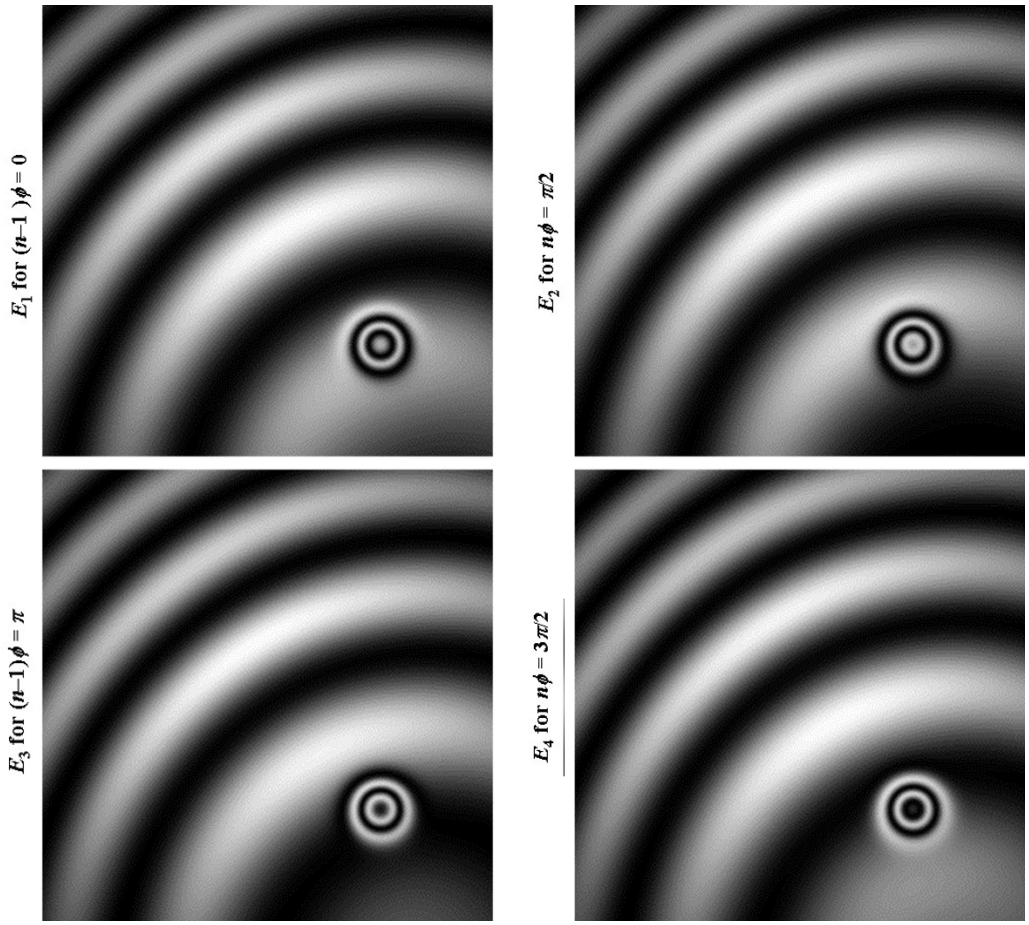

Figure 14 : phase shifted interferograms

As we have seen previously, the phase can be calculated using the following relation:

$$\Delta\varphi = \arctan\left(\frac{E_4 - E_2}{E_1 - E_3}\right)$$

Figure 15 shows the results obtained after applying the algorithm to the 4 shifted interferograms.

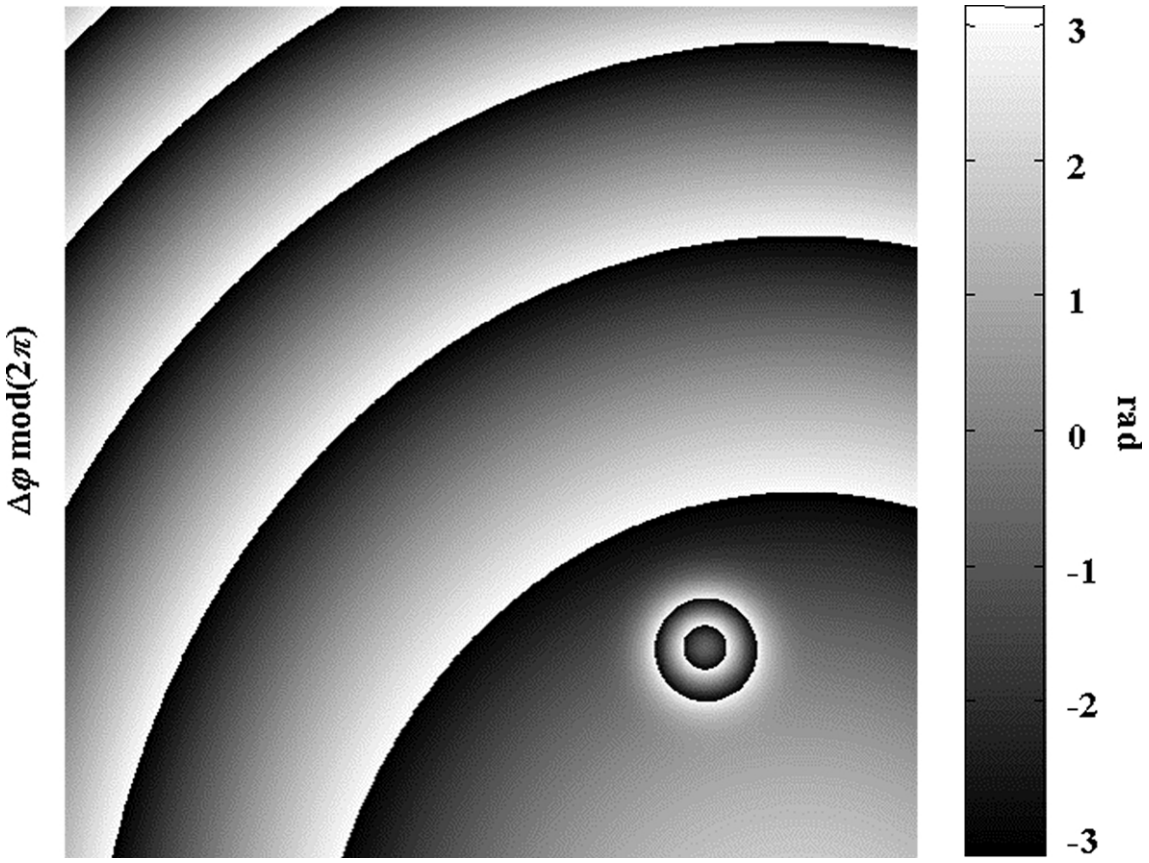

Figure 15 : wrapped phase estimated usinf the 4 shifted interferograms

The phase is only obtained modulo 2π, thus producing the phase jumps observed on the figure. When we apply a phase unwrapping algorithm, we obtain the result shown on figure 16.

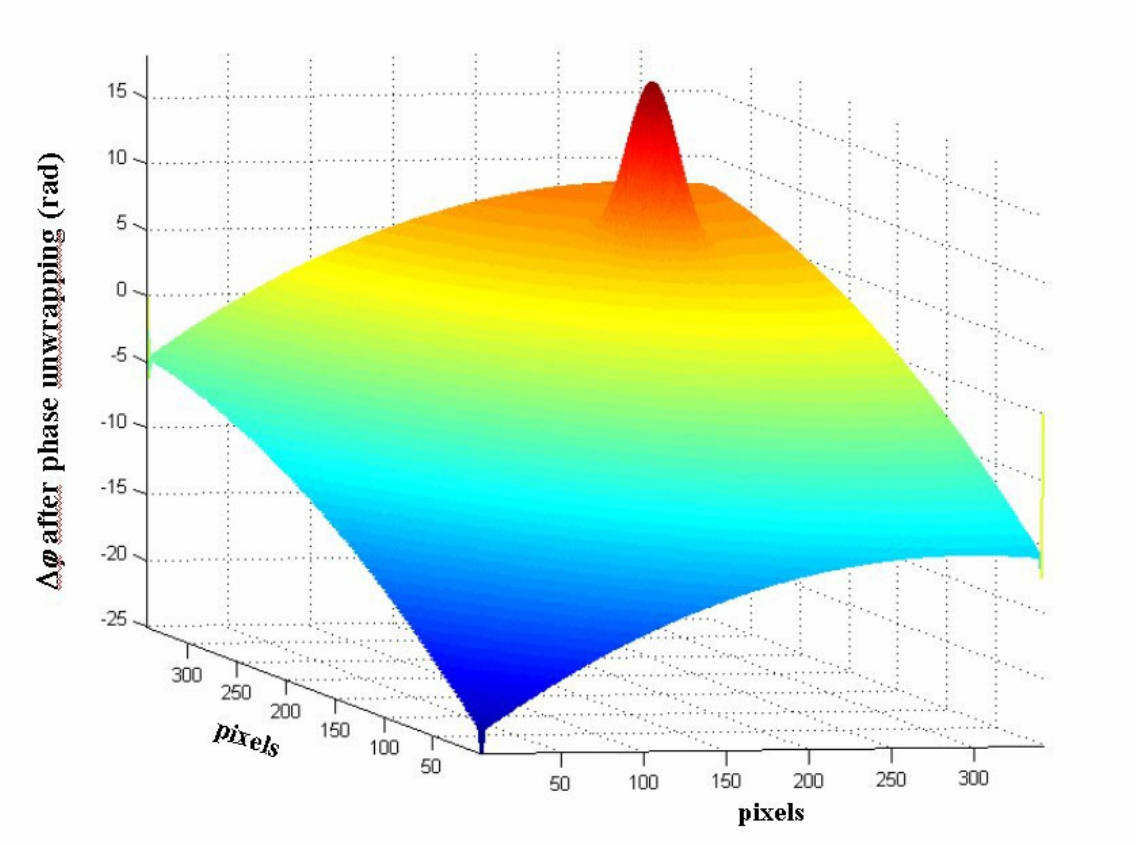

Figure 16 : unwrapped phase

The reader will note that the 0 value of the phase measurement is arbitrary and depends on the starting point of the phase unwrapping algorithm. This level can therefore be adjusted if it is possible to know a point in the phase map where the phase is really equal to 0.

3. Phase demodulation with spatial carrier

3.1. Fourier transform demodulation

This method was introduced in 1982 [11 [[11]]], and was originally used in one dimension with monodimensional FFT algorithms, before evolving towards a bidimensional form with the introduction of fast FFT2 algorithms. In both cases, after Fourier transforming the fringe pattern, we obtain a tri-modal spectrum having symmetry with respect to the origin.

This method offers the big advantage of significantly reducing the noise level of the demodulated phase map, but degrades the spatial resolution. The phase modulation is purely spatial [11 [[11]]] :

$$\zeta(x, y, t) = 2\pi u_0 x + 2\pi v_0 y$$

We can consider the cases where $u_0 = 0$ or $v_0 = 0$; the principle of the method stays valid. In the following, we will consider the latter case.

The choice of the spatial carrier must take into account the number of pixels and the horizontal and vertical sampling periods of the CCD camera. If we note p_x and p_y the pixel sizes of the CCD camera, then the sampling frequencies are $f_x = 1/p_x$ and $f_y = 1/p_y$. In practice, we also

need to take into account the **Modulation Transfer Function** (MTF) of the imaging optical system associated with the CCD camera.

The carrier frequency should verify Shannon theorem: $u_0 < f_x/2$ and $v_0 < f_y/2$. In the Fourier plane of the interferogram, the frequency step between two spectral values is of $_x/N$ horizontally and f_y/M vertically where N and M are the number of pixels of the image matrix (without zero-padding the interferogram).

To obtain a spatial carrier centered at $f_x/4$ (resp. $f_y/4$), i.e. in the middle of the window of positive frequencies, the spatial period of the carrier must be equal to $1/u_0 = 4p_x$(resp. $1/v_0 = 4p_y$) and each fringe must cover 4 pixels on the camera. The total number of fringes is therefore about $N/4$ (resp. $M/4$).

The fringe pattern registered at the detector can be written:

$$E(x,y)=a(x,y)+b(x,y)\cos(\Delta\varphi(x,y)+2\,\pi\,u_0 x)$$

We can rewrite this expression by introducing complex exponential functions and by taking into account the spatial dependency:

$$E(x,y)=a(x,y)+\frac{1}{2}b(x,y)\exp(i\Delta\varphi(x,y))\exp(2\,i\,\pi\,u_0 x)$$
$$+\frac{1}{2}b(x,y)\exp(-i\Delta\varphi(x,y))\exp(-2\,i\,\pi\,u_0 x)$$

We note $c(x,y) = \frac{1}{2}b(x,y)\,exp\,(i\Delta\varphi(x,y))$ and we apply a Fourier transform to the registered image:

$$\widetilde{E}(u,v)=\widetilde{A}(u,v)+\widetilde{C}(u-u_0,v)+\bar{\widetilde{C}}(u+u_0,v)$$

where

$$\widetilde{A}(u,v)=TF[a(x,y)](u,v)$$
$$\widetilde{C}(u,v)=TF[c(x,y)](u,v)$$

and $\bar{\widetilde{C}}(u,v)$ is the complex conjugate of $\widetilde{C}(u,v)$

If the spatial frequency spectra are narrow compared to the carrier frequency u_0, we observe three separate peaks in the Fourier plane of the interferogram. The two symmetrical peaks centered at $+u_0$and $-u_0$contain the same phase information. They are simply complex conjugated. Spatially filtering of the peak centered at $+u_0$, , using a bidimensional digital bandpass filter centered at $+u_0$, enables extracting the phase information we are interested in and also removing the continuous component.

We note $\widetilde{H}(u,v)$ the transfer function of the filter. The filter is applied to the spectrum by multiplying the Fourier transform of the image with this transfer function. We have:

$$\widetilde{E}_f(u,v)=\widetilde{E}(u,v)\widetilde{H}(u,v)\simeq\widetilde{C}(u-u_0,v)$$

The filter can be easily described using a **"bidimensional rectangular function" of widths** Δu and Δv :

$$\widetilde{H}(u,v)=\begin{pmatrix}1 & \text{if } \{u,v\}\in[u_0-\Delta u/2,u_0+\Delta u/2]\times[-\Delta v/2,\Delta v/2]\\ 0 & \text{sinon}\end{pmatrix}$$

Applying an inverse Fourier transform to $\widetilde{E_f}(u,v)$ gives:

$$c_f(x,y)=\frac{1}{2}b(x,y)\exp(i\Delta\varphi(x,y))\exp(2\,i\,\pi\,u_0 x)$$

By multiplying $c_f(x,y)$ with $exp(-2i\pi u_0 x)$ we obtain:

$$\widetilde{c}(x,y)\simeq\frac{1}{2}b(x,y)\exp(i\Delta\varphi(x,y))$$

and we can deduce the optical phase by using an arctangent function:

$$\Delta\varphi(x,y)=\arctan\left(\frac{\Im(\hat{c})}{\Re(\hat{c})}\right)$$

The reader will note that this filtering can also be implemented in the real space, by convolution of the interferogram with the filter. Indeed, since:

$$\widetilde{E}_f(u,v)=\widetilde{E}(u,v)\widetilde{H}(u,v)\simeq\widetilde{C}(u-u_0,v)$$

we also have in the real space:

$$c_f(x,y)=E(x,y)*h(x,y)$$

where:

$$h(x,y)=\mathrm{TF}^{-1}[\widetilde{H}(u,v)](x,y)$$

giving:

$$h(x,y)=\Delta_u\Delta_v\exp(-2\,i\,\pi\,u_0 x)\,\mathrm{sinc}(\pi\Delta_u x)\,\mathrm{sinc}(\pi\Delta_v y)$$

Digital filtering can be implemented using a 2 dimensional linear filter of size $K\times K$ and of finite impulse response:

$$h(k,l)=\begin{pmatrix}p_x p_y\Delta_u\Delta_v\exp(-2\,i\,\pi\,u_0\,p_x k)\,\mathrm{sinc}(\pi\Delta_u p_x k)\,\mathrm{sinc}(\pi\Delta_v p_y l)\\ \text{for}\{k,l\}\in[-L,+L]\times[-L,+L]\\ 0 \quad \text{sinon}\end{pmatrix}$$

where $L=(K-1)/2$.

The spatial resolution of this method is strongly dependent of the filter widths. If we note (R_x, R_y) the widths at the first zero of the impulse response function, then the spatial resolution is given by:

$$R_x = 1/\Delta_u$$
$$R_y = 1/\Delta_v$$

We therefore conclude that we should increase as much as possible the filter bandpass while making sure that there is no contribution from the other peaks after filtering.

The reader will note that even though the two formulations (spectral and spatial filtering) are mathematically equivalent, their digital implementation will give different results.

Indeed, synthesizing the digital filter of finite impulse response necessarily imposes to truncate the number of coefficients since the impulse response must be finite. This truncation introduces oscillations in the passband and in the attenuated band of the filter. Therefore, since unwanted spectral regions can coincide with these oscillations, this filtering is less selective than spectral filtering for which the selected spectral region are directly extracted in the Fourier plane.

This method is very robust if the signal to noise ratio of the biased interferogram is very high. Otherwise, even though filtering strongly reduces the noise level, some problems linked to fringe breaking might appear in the processed phase map. This is also true if the fringe pattern modulation includes a multiplicative noise, as it is the case for speckle interferometry, for example. In this case, phase unwrapping is challenging.

Remarque

These algorithmic formulations assume that we know perfectly well the value of the carrier frequency. This assumption is easy to fulfill if the interferogram is not too noisy or if the fringe pattern modulation stays perfectly uniform within the image. Otherwise, estimating the carrier frequency is not so easy and a bad estimation can lead to artifacts in the optical phase (introduction of a phase tilt). Selecting the central peak requires a strong interaction with the user for the selection to be reliable. Complete automation of the processing is therefore very complicated.

3.2. Phase shifting with spatial carrier

In this method, a spatial frequency carrier is also introduced:

$$\zeta(x, y, t) = 2\pi v_0 y \qquad \text{or} \qquad \zeta(x, y, t) = 2\pi u_0 x$$

which value is perfectly known from one pixel to its neighbor. In the previous case, we sought to increase the carrier frequency as much as possible without worrying about its value in the acceptable limit where the three peaks in the Fourier domain where well separated.

The method we are describing here uses a spatial carrier that must be perfectly known, such that the phase variation over a distance of K adjacent pixels (horizontal or vertical) is equal to 2π [12 [[12]]]. We therefore assume that within a region of K pixels, the phase $\Delta\varphi$ and the interferogram parameters $a(x, y)$ and $b(x, y)$ stay constant.

Let us consider the case where $\zeta(x, y, t) = 2\pi u_0 x$ with a phase difference of $2\pi/L$ between two adjacent pixels; we then have $2\pi u_0 p_x = 2\pi/L$ i.e. $1/u_0 = L\, p_x$:

we therefore have L pixels per fringe.

The principle of this method is to locally sample the sinusoidal signal in K points represented by K adjacent pixels, with a phase difference of $2\pi/L$ between two adjacent pixels.

Using a unique image, we synthesize, by spatial undersampling, K secondary images by considering for each image only the pixel #k of the K pixels. If the initial image matrix

contains M rows and N columns, then each secondary image will contain M rows and $1+(N-1)/K$ columns.

Using a spatial carrier oriented along the *x* axis, the interferogram can be written, as a function of the pixel position:

$$
\begin{aligned}
&E(x,y)=a(x,y)+b(x,y)\cos(\Delta\varphi(x,y)+2\pi u_0 x)\\
&E(x+p_x,y)\approx a(x,y)+b(x,y)\cos(\Delta\varphi(x,y)+2\pi u_0 x+2\pi/L)\\
&E(x+2p_x,y)\approx a(x,y)+b(x,y)\cos(\Delta\varphi(x,y)+2\pi u_0 x+4\pi/L)\\
&\vdots\\
&E(x+Mp_x,y)\approx a(x,y)+b(x,y)\cos(\Delta\varphi(x,y)+2\pi u_0 x+2(K-1)\pi/L)
\end{aligned}
$$

Using pixels from $E(x,y)$, $x \in [x_{min}, x_{max}]$ with steps of Kp_x we form image E_1 ;
Using pixels from $E(x,y)$, $x \in [x_{min}+p_x, x_{max}]$ with steps of Kp_x we form image E_2; etc. ;
Using pixels from $E(x,y)$, $x \in [x_{min}+(K-1)p_x, x_{max}]$ with steps of Kp_x, we form image E_K ;
Figure 17 illustrates the principle of pixel selection along each row of the primary interferogram.

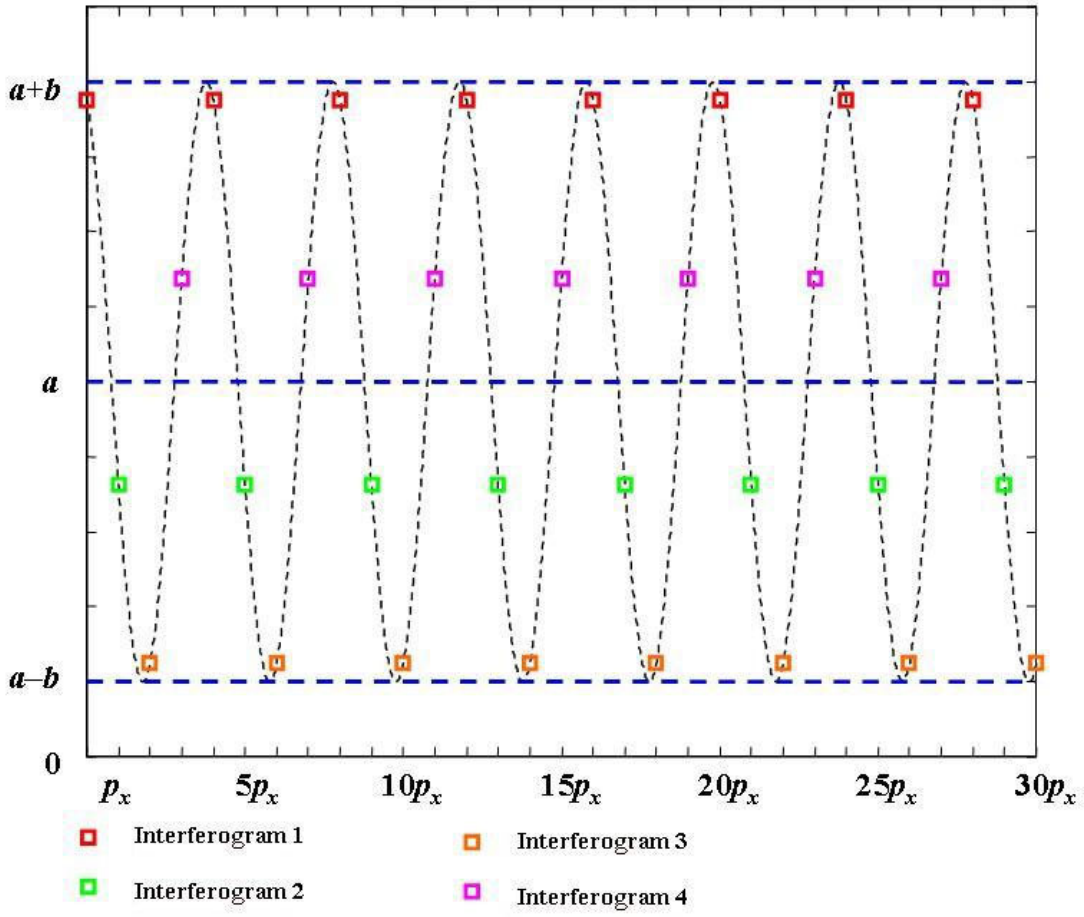

Figure 17 : principle of pixel selection

For example, if we consider the case where $K = 3$ and $L = 3$, we have $2\pi u_0 p_x = 2\pi/3$ i.e $u_0 = 1/3p_x$. , i.e. 3 pixels per fringe. For the secondary images, we have:

$$\begin{aligned} E_1 &= a + b\cos(\Delta\varphi + 2\pi u_0 x) && \text{extracted from} && E(x,y) \\ E_2 &= a + b\cos(\Delta\varphi + 2\pi u_0 x + 2\pi/3) && \text{extracted from} && E(x+p_x,y) \\ E_3 &= a + b\cos(\Delta\varphi + 2\pi u_0 x + 4\pi/3) && \text{extracted from} && E(x+2p_x,y) \end{aligned}$$

and the phase is given modulo 2π by:

$$\Delta\varphi + 2\pi u_0 x = \arctan\left(\frac{3}{\sqrt{3}}\frac{E_3 - E_2}{2E_1 - E_2 - E_3}\right)$$

The phase is then uwrapped and the term corresponding to the spatial carrier is removed.

3.3. Spatial lock-in demodulation

This method is similar to conventional lock-in demodulation, with the particularity that a carrier frequency is introduced in the fringe pattern. For a horizontal carrier, the biased interferogram registered on the detector can be written:

$$E(x,y) = a(x,y) + b(x,y)\cos(\Delta\varphi(x,y) + 2\pi u_0 x)$$

Spatial lock-in detection consists in multiplying, in the spatial domain (x,y), the biased interferogram with a carrier of same frequency, but without a constant term:

- on one hand in phase with the interferogram [13 [[13]]]
- on the other hand in quadrature with the interferogram [13 [[13]]]

We consider a spatial carrier of same frequency and phase than the interferogram:

$$P(x,y) = \cos(2\pi u_0 x)$$

and the same carrier in quadrature

$$Q(x,y) = \sin(2\pi u_0 x)$$

Multiplying $E(x,y)$ with $P(x,y)$ gives

$$EP(x,y) = a(x,y)\cos(2\pi u_0 x) + \frac{1}{2}b(x,y)\cos(\Delta\varphi(x,y) + 4\pi u_0 x) + \frac{1}{2}b(x,y)\cos(\Delta\varphi(x,y))$$

$EP(x,y)$ is composed of three terms: two of high spatial frequency content ($2\pi u_0 x$ and $4\pi u_0 x$) and of one low-frequency term which carries the information on the wanted phase.

By spatially filtering EP with a low pass filter centered at frequency $(u,v) = (0,0)$ of widths Δu and Δv , and transfer function:

$$\tilde{H}(u,v) = \begin{pmatrix} 1 & \text{if } \{u,v\} \in [-\Delta u/2, +\Delta u/2] \times [-\Delta v/2, \Delta v/2] \\ 0 & \text{sinon} \end{pmatrix}$$

and of impulse response:

$$h(x,y)=\Delta_u \Delta_v \mathrm{sinc}(\pi \Delta_u x)\mathrm{sinc}(\pi \Delta_v y)$$

we obtain:

$$M_1(x,y)=EP(x,y)*h(x,y)=\frac{1}{2}b(x,y)\cos(\Delta\varphi(x,y))$$

We apply the same process to the biased interferogram multiplied with the phase shifted carrier,

$$EQ(x,y)=a(x,y)\sin(2\pi u_0 x)+\frac{1}{2}b(x,y)\sin(\Delta\varphi(x,y)+4\pi u_0 x)$$
$$+\frac{1}{2}b(x,y)\sin(\Delta\varphi(x,y))$$

and after filtering we get:

$$M_2(x,y)=EQ(x,y)*h(x,y)=\frac{1}{2}b(x,y)\sin(\Delta\varphi(x,y))$$

The phase is therefore obtained with an arctangent function:

$$\Delta\varphi=\arctan\left(\frac{M_2(x,y)}{M_1(x,y)}\right)$$

and the fringe pattern modulation amplitude is given by:

$$b(x,y)=4\sqrt{M_1^2(x,y)+M_2^2(x,y)}$$

The lowpass filter must have a spatial bandwidth wide enough to keep the useful spectrum but not too wide in order to fully reject the frequency components of the side peaks.

3.4. Illustrations

We consider again the interferogram of figure 13. This interferogram is said to be "**un-biased**" in the sense that it doesn't contain any intently added spatial carrier.

We now introduce a spatial carrier of spatial frequency $u_0 = 1/4p_x$. The resulting biased interferogram is observed on figure 18.

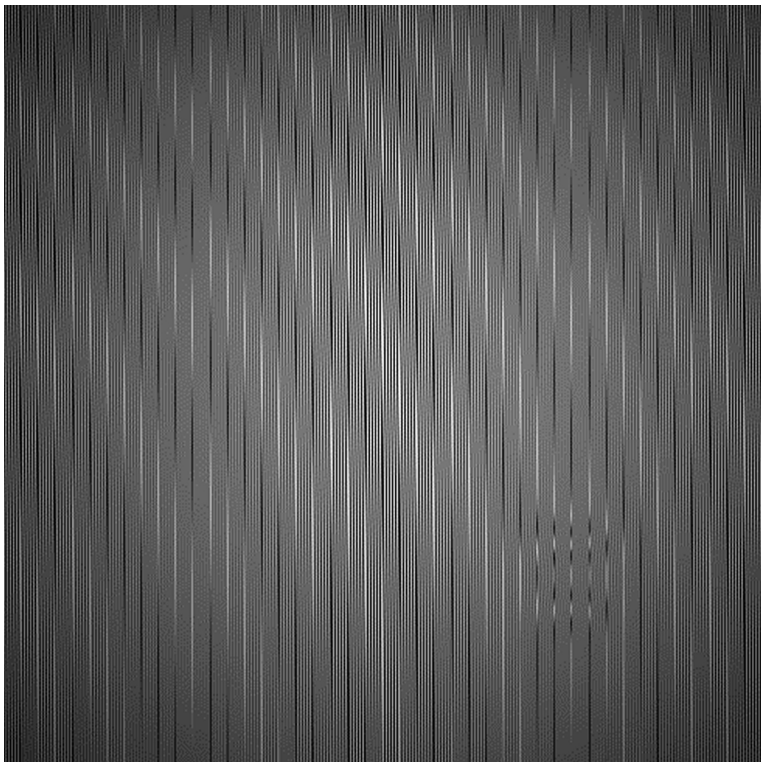

Figure 18 : biased interferogram

Figure 19 shows the spectrum of the biased interferogram. We can observe its trimodal composition. The useful region to extract has been framed in red.

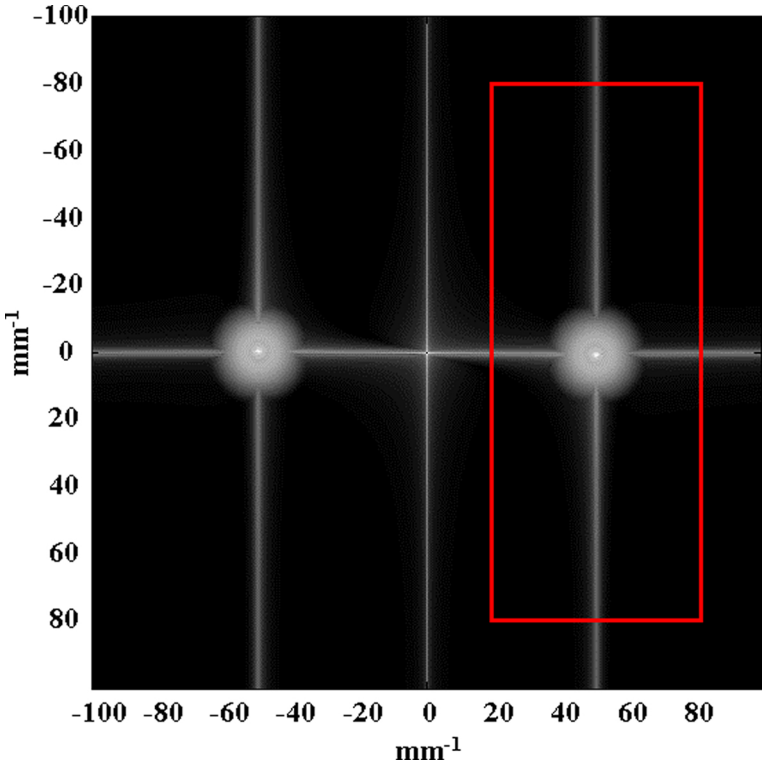

Figure 19 : spectrum of the biased interferogram

The useful region being defined, the digital filtering mask $\widetilde{H}(u,v)$ is built by assigning the value of 1 to the useful region and of 0 to the region to filter out. Figure 20 shows the filtering mask of the spectrum shown in figure 19.

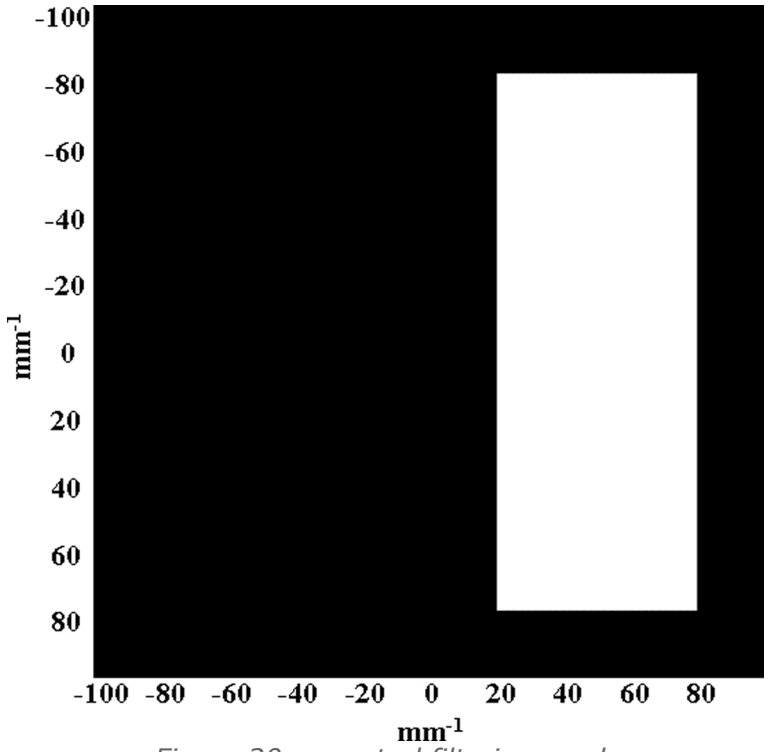

Figure 20 : spectral filtering mask

Figure 21 shows the phase calculated modulo 2π after applying the method described above.

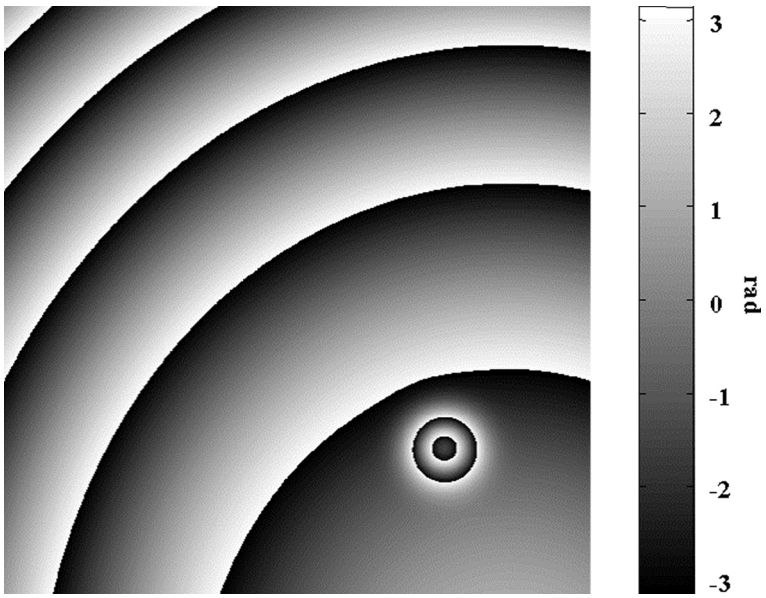

Figure 21 : phase calculated by applying the above method

Since the spatial frequency was chosen such that $u_0 = 1/4p_x$, it is also possible to apply the spatial phase shifting method with 4 secondary interferograms extracted from the biased interferogram. Figure 22 shows the 4 interferograms.

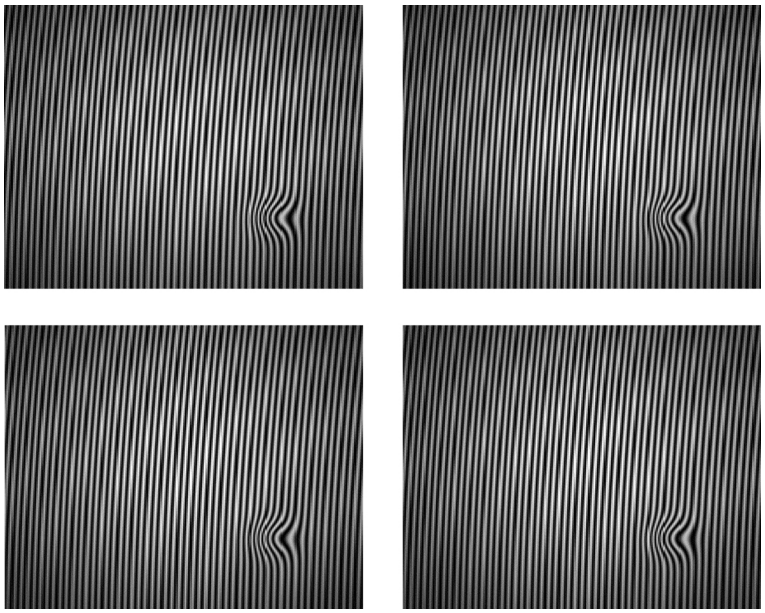

Figure 22 : interferograms extracted from the primary interferogram

The phase is estimated with the 4-images algorithm previously described. The result is shown on figure 23.

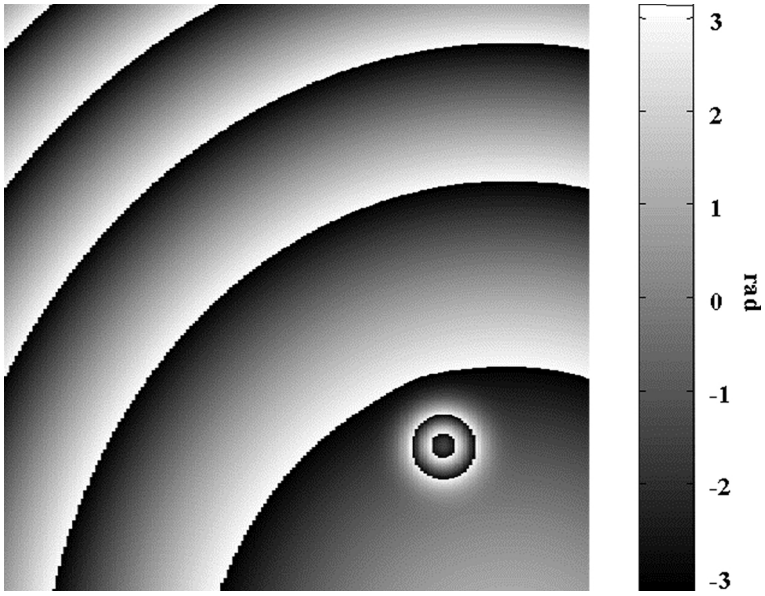

Figure 23 : phase estimated by spatial phase shifting

Figure 24 shows three profiles of the phase map obtained after phase unwrapping.

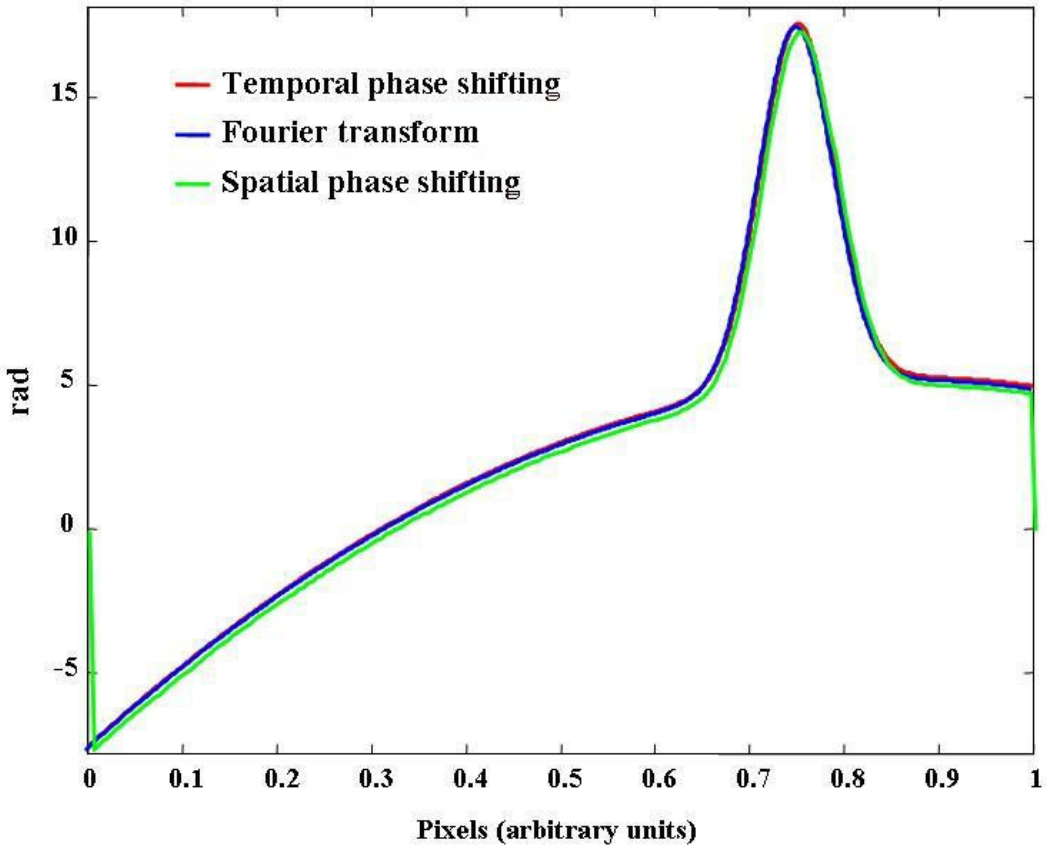

Figure 24 : phase obtained after unwrapped

We note the good agreement between the three profiles.

3.5. Spatial phase modulation techniques

The spatial carrier is usually introduced with a controlled inclination of one of the wave surface of the interferometer. It is therefore possible to choose the carrier orientation (x, y or both).

Diffraction gratings can also be used, which introduce an inclination of the diffracted wave. The grating is chosen according to the targeted carrier spatial frequency.

III.Etude de cas

Among all possible applications of fringe pattern demodulation techniques, we have chosen to illustrate the case of **speckle interferometry**[14 [[14]],15 [[15]]]. This method is extremely interesting to study the behavior of structures or mechanical assembly exposed to solicitations such as mechanical, pneumatic, thermal or acoustic loading.

The speckle phenomenon appears when a naturally rough surface is illuminated with spatially and temporally coherent light (usually from a laser).

The statistical properties of speckle usually depend on the **coherence of the incident beam** and on the **statistical properties of the diffusing surface** (or medium). In the case where speckle is produced with a highly coherent light illuminating a large diffusing surface, speckle statistics do not depend on the surface properties and we talk about **"normal speckle pattern"** . However, in general, speckle statistics depend both on the light coherence and the diffuser nature.

The principle of speckle interferometry is to register not only the speckle amplitude but also the phase variation before and after object distortion. The coding is based on the coherent superposition of a speckle pattern with a reference wave without speckle, or with another speckle wave coming from the same object or from another reference object.

1. Experimental setup

Figure 1 shows a speckle interferometry setup used to study the watertightness of an industrial connector of area $15 \times 23\ mm^2$.

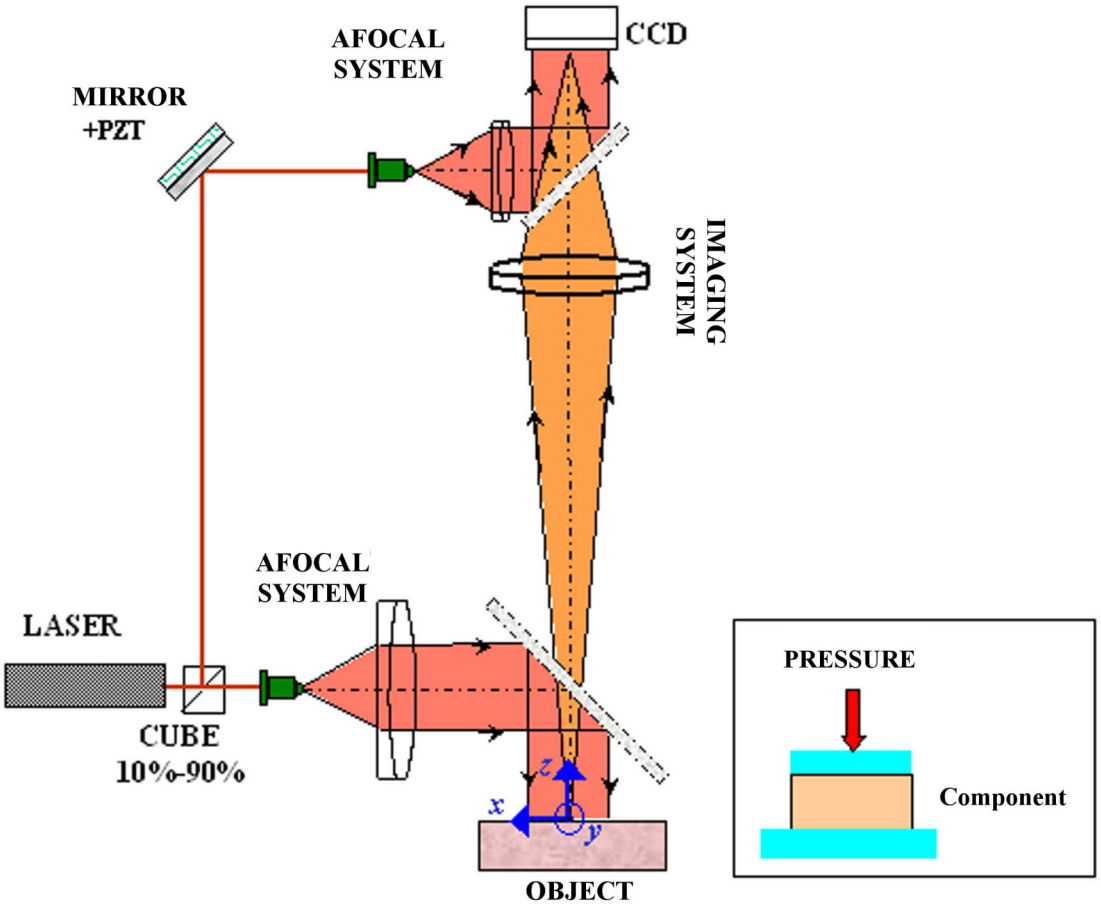

Figure 1 : Speckle interfermoter

The interferometer is composed of a laser source, $\lambda = 0.6328\ \mu m$, which is separated into two beams with a ratio $10\% - 90\%$. The beam illuminating the object is collimated and at normal incidence to the object surface. The object diffracts a wave towards the image sensor. The imaging objective, of f-number $N = 8$, images the object surface on the detector with a transverse magnification of g_x. The detector is a CCD (Charge Coupled Device) camera containing 572×768 pixels of size $p_x \times p_y = 8.6 \times 8.6\ \mu m^2$. The detector encodes the image with 8 bits and each pixel has a full well capacity of $N_e = 30000\ electrons$ and an electronic noise of 10 electrons.

The reference beam interferes with the object beam at the detector. On the reference beam path, a mirror is mounted on a piezo-electric device of sensitivity $s_{pzt} = 0.25\ \mu m/V$. This sensitivity has been estimated with a precision of $\sigma_{pzt}/s_{pzt} = 5\%$. The image of the object, observed through the objective, is superimposed with the speckle pattern due to coherent illumination and to the natural roughness of the object. This image is shown on figure 2.

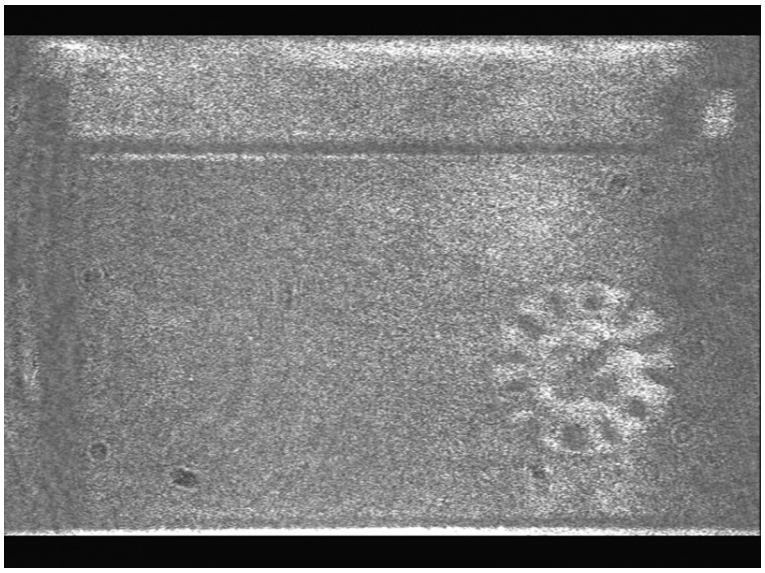

Figure 2 : image of the object

This image is of bad quality because of the speckle grains which constitute a coherent noise of random fluctuation. However, the random pattern encodes for a (random) interference signal since the speckle interferes with the reference wave. The signal registered on the sensor takes the following expression:

$$E(x,y)=a(x,y)+b(x,y)\cos(\psi(x,y))$$

The optical phase ψ is random and uniformly distributed over $[-\pi,+\pi]$. In the sensor plane, the speckle has a (statistical) mean length given by:

$\phi_{xy} = 1.22\lambda N(1-g_y)$ *in the plane* (x,y)

$\Delta z = 8\lambda N^2(1-g_y)^2$ along the propagation axis.

The two numbers constitute the transverse and axial correlation lengths of the speckle in the image plane.

Using the numerical value, $g_y = -0.28$, we obtain $\phi_{xy} = 7.9\ \mu m$ and $\Delta z = 530\ \mu m$. The size of a speckle grain in the image plane is therefore on the order of $8\ \mu m$, and we have approximately one speckle grain per pixel. This value indicates that the maximum speckle shift that can be measured with this process is smaller than $8\ \mu m$.

Considering that the random fluctuation have a correlation length equal to the pixel size, we can infer that any spatial filtering with a kernel of several pixels will strongly reduce that fluctuation.

2. Principle of the measurement

To evaluate the watertightness of the component, we measure the deformation obtained when the component is under compression (see figure 1).

If we note $\delta(x,y)$ the deformation of the component surface between two instants corresponding to two different loadings, the variation of optical phase produced by the surface displacement can be expressed:

$$\Delta\varphi(x,y)=\frac{4\pi}{\lambda}\delta(x,y)$$

Therefore, the interferometric signal is modified by the phase variation. After loading, we have:

$$F(x,y)=a(x,y)+b(x,y)\cos(\psi(x,y)+\Delta\varphi(x,y))$$

The reader will note that since the speckle signal and its random phase are still present in the signal, the image F is also very noisy and observing $\Delta\varphi$ is impossible.

Considering the expressions of E and F, the final interference pattern can be easily deduced from the initial pattern. Indeed, when $\Delta\varphi = 2k\pi$ the two patterns are identical and $E = F$. Within a complete cycle of variation of $\Delta\varphi$ between $2k\pi$ and $2(k+1)\pi$ the two patterns progressively decorrelate and reach a maximum of decorrelation for $\Delta\varphi = 2(k+0.5)\pi$.

Therefore, by comparing the two patterns it will be possible to recognize the identical regions, i.e. to visualize the lines or regions where the speckle grains have been modified on the same manner by the object distortion.

This is true at the condition that the speckle doesn't change too much when the object is being loaded. The speckle patterns obtained with the two loads must be correlated, which means that the displacement produced at the object surface must be smaller than the speckle grain correlation length $(\phi_{xy}, \Delta z)$.

3. Correlation fringes

The techniques enables the visualization of the object displacements by simple geometric superposition (similarly to moiré techniques). Since the speckle patterns are registered using a CCD camera, it is possible to digitally compare reference E to deformation F. We subtract in real time the reference image to the current image and we display the modulus of the result:

$$\Delta E=|F-E|=4b\left|\sin\left(\frac{\Delta\varphi}{2}\right)\right|\left|\sin\left(\psi+\frac{\Delta\varphi}{2}\right)\right|$$

Figure 3 shows the results obtained with this technique.

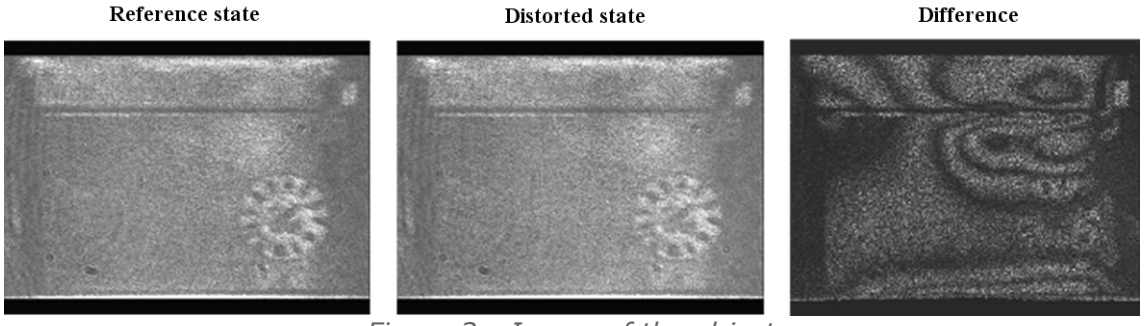

Figure 3 : Image of the object

We observe the correlation fringes, which correspond to the line of equal displacement of the structure between the two loadings.

4. Phase demodulation

Observing the correlation fringes is very useful for the engineer to understand how the component is distorted and to infer its watertightness defaults. However, it is only an observation method, not quantitative. The observed signal being of interferometric nature, it is

possible to demodulate the random phase and to extract the phase variation between the two loadings. Since the experimental setup includes a piezoelectric transducer, it will be possible to apply the technique of temporal phase stepping.

We consider the acquisition of 4 images in the reference state:

$$E_1 = a + b\cos(\psi)$$

$$E_2 = a + b\cos(\psi + \frac{\pi}{2})$$

$$E_3 = a + b\cos(\psi + \pi)$$

$$E_4 = a + b\cos(\psi + \frac{3\pi}{2})$$

Considering the geometry and sensitivity of the piezoelectric device, a phase step of $\pi/2$ is obtained for a mirror displacement of $\lambda/4\sqrt{2}$, i.e. 111.86 nm, which corresponds to a voltage of 27.96 mV.

The 4 inteferograms enable the recovering of the phase by applying the suitable algorithm:

$$\varphi_1 = \psi = \text{atan}\left(\frac{E_4 - E_2}{E_1 - E_3}\right)$$

We repeat the same operation after loading of the object:

$$F_1 = a + b\cos(\psi + \Delta\varphi)$$

$$F_2 = a + b\cos(\psi + \Delta\varphi + \frac{\pi}{2})$$

$$F_3 = a + b\cos(\psi + \Delta\varphi + \pi)$$

$$F_4 = a + b\cos(\psi + \Delta\varphi + \frac{3\pi}{2})$$

We now obtain :

$$\varphi_2 = \psi + \Delta\varphi = \text{atan}\left(\frac{F_4 - F_2}{F_1 - F_3}\right)$$

The phase variation due to the object distorsion is estimated by calculating:

$$\widehat{\Delta\varphi} = \varphi_2 - \varphi_1$$

The phase variation due to the object distorsion is estimated by calculating:

$$\widehat{\Delta\varphi} = \operatorname{atan}\left(\frac{(F_4 - F_2)(E_1 - E_3) - (F_1 - F_3)(E_4 - E_2)}{(F_1 - F_3)(E_1 - E_3) + (F_4 - F_2)(E_4 - E_2)}\right)$$

Figure 4 shows the two phases extracted by applying the algorithm to the two sets of interferograms.

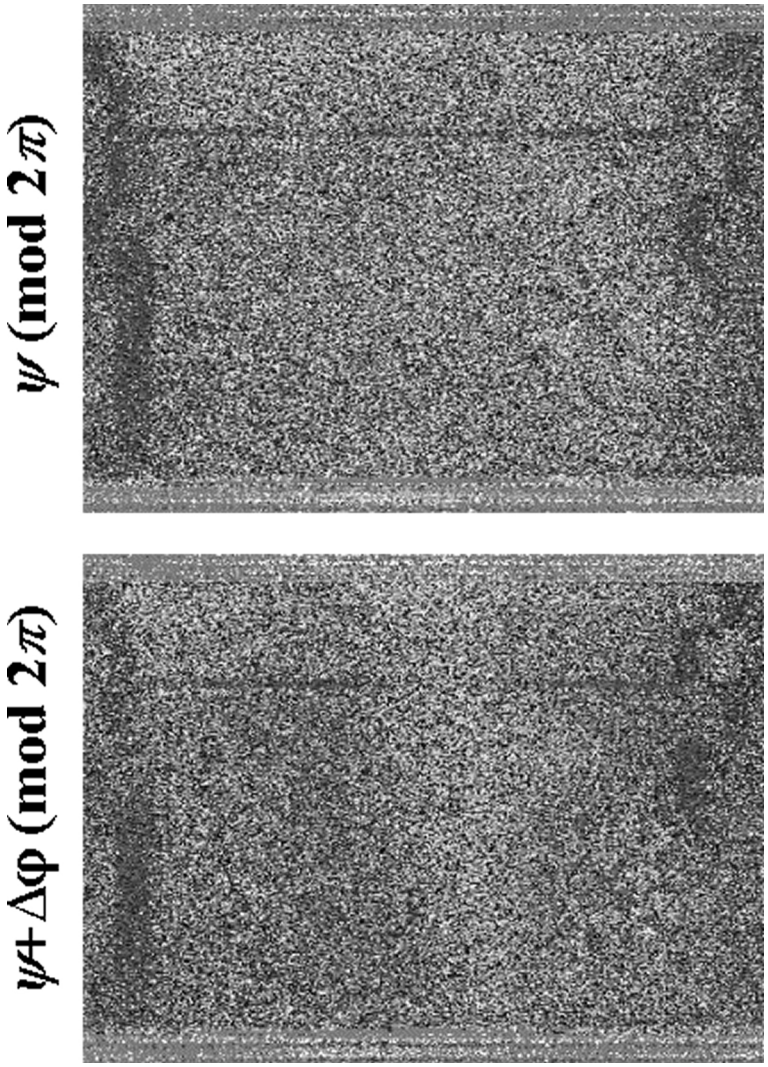

Figure 4 : phase measurement

We notice the random nature of the two phase measurements. Figure 5 shows the phase variation modulo 2π estimated using the set of 2×4 shifted interferograms.

Figure 5 : phase variation due to the load

Note that the map obtained with this technique is noisy. Indeed, the loading induces a displacement of the speckle which starts to decorrelate, thus introducing random fluctuations in the second set of interferograms. These fluctuations appear in the measurement of the phase variation.

Processing this map thus requires **digital filtering**. In practice, filtering is not applied to $\Delta\varphi$ because it would destroy the phase steps of 2π that can be observed on figure 5, but rather to $sin(\Delta\varphi)$ and $cos(\Delta\varphi)$ which are smooth functions, contrary to arctangent which presents some discontinuities. The filter is usually a mean filter or median filter with a sliding window of $3\times3, 5\times5$, or 7×7. The kernel size must be adapted to the desired spatial resolution in the image plane. We can consider that linear filtering with a kernel KK degrades the resolution by Kp_x. Figure 6 shows the phase map filtered with a mean filter of kernel size $K = 7$ applied to the cosine and sine functions of the phase variation.

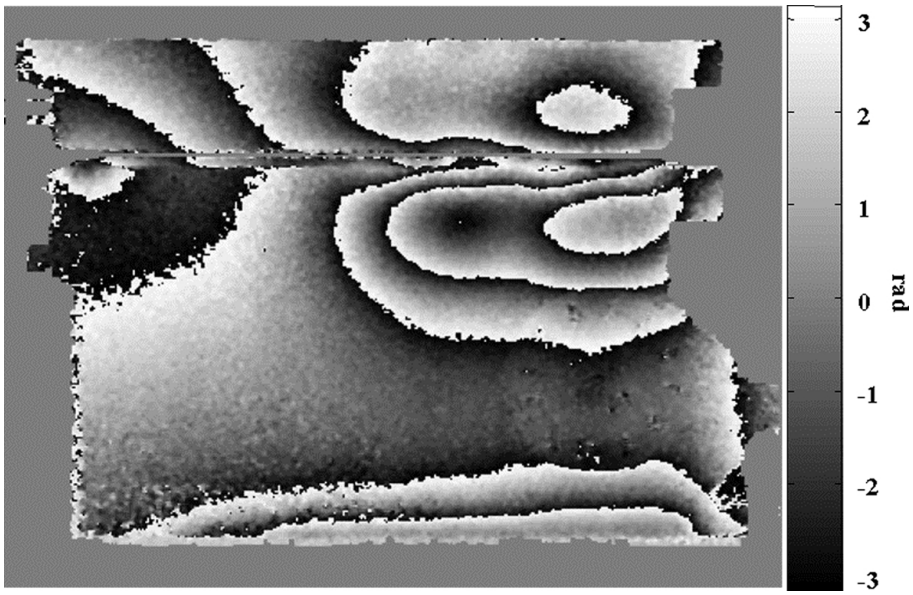

Figure 6 : smoothed phase variation

Note that the random fluctuations have almost completely disappeared. This type of filtering is always necessary in speckle interferometry.

The phase map can now be unwrapped to remake 2π phase jumps. Figure 7 shows the result after unwrapping.

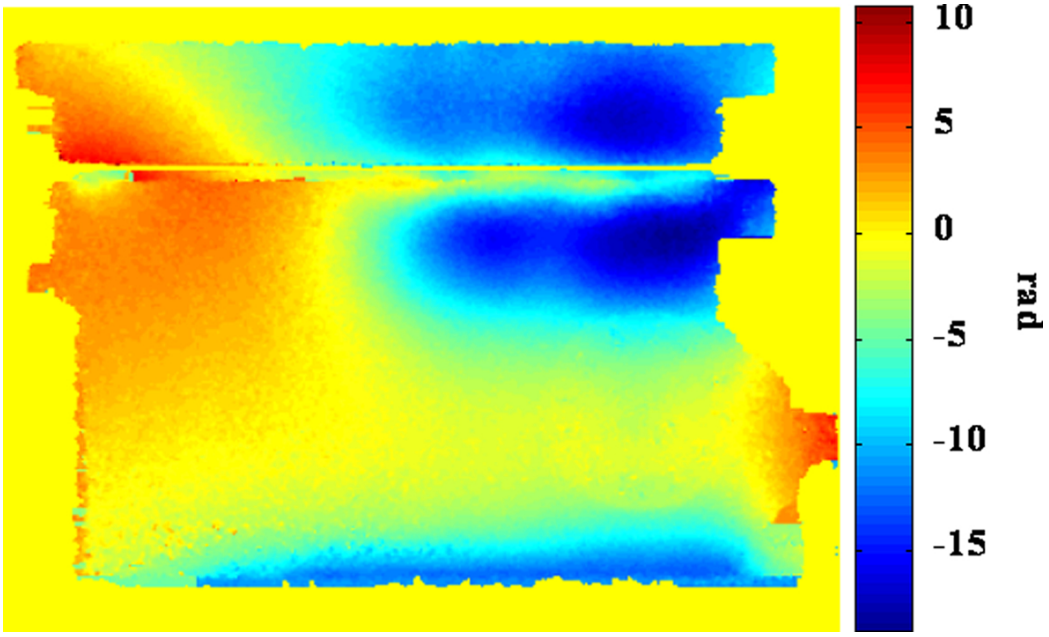

Figure 7 : unwrapped phase variation

In the case of the watertightness study, loading is applied until reaching $33\,\mu m$ of displacement. By applying the previous procedure, and by summing the intermediate results, we can build a map of the object distortion between loading "0" and loading "$33\,\mu m$". Figure 8 shows the result.

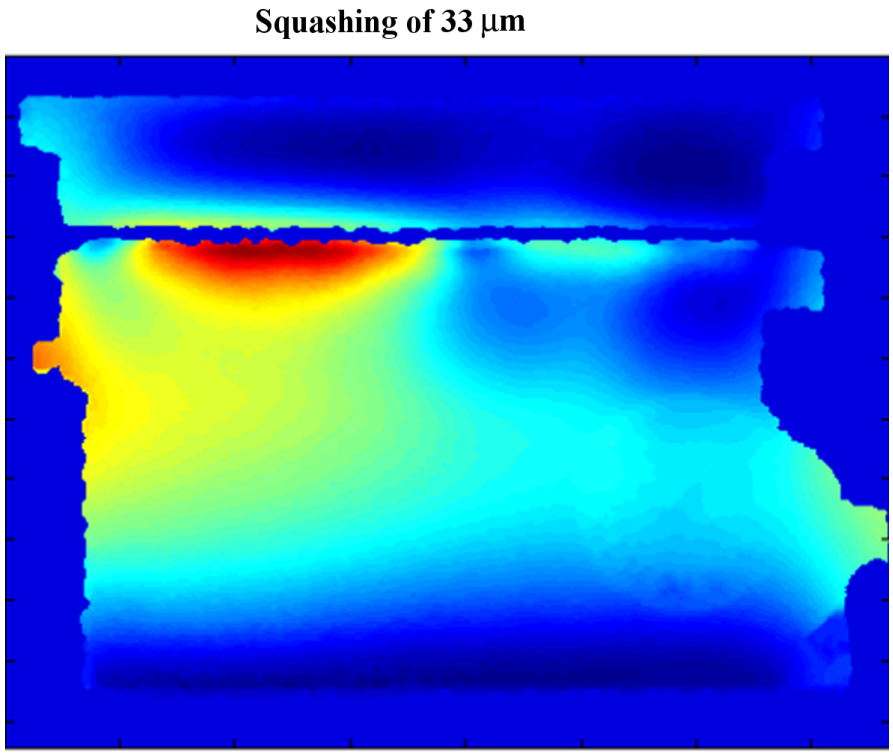

Figure 8 : measurement of the object disortion under a loading corresponding to a a displacement of 33 mm

When describing the interferometric process, we chose to use an algorithm with 24, interferograms shifted by $\pi/2$. This choice represents a good comprise between robustness to random fluctuations and speed of acquisition and digital processing. Intuitively, we can think that the robustness to noise improves when the number of interferograms is increased.

For example, we can use a subset of the previous set of interferograms composed of only 22 interferograms shifted by $\pi/2$. The algorithm, which we haven't introduced in the lesson, has been specially developed for speckle interferometry. The phase variation is estimated by:

$$\widehat{\Delta\varphi} = -\frac{\pi}{2} - 2\arctan\left(\frac{E_1 - F_2}{E_2 - F_1}\right)$$

We can also use 23, interferograms shifted by $\pi/2$, from the same set of interferograms. The reader can show that the corresponding algorithm reads:

$$\widehat{\Delta\varphi} = \arctan\left(\frac{(2F_2 - F_1 - F_3)(E_3 - E_1) - (2E_2 - E_1 - E_3)(F_3 - F_1)}{(F_3 - F_1)(E_3 - E_1) + (2F_2 - F_1 - F_3)(2E_2 - E_1 - E_3)}\right)$$

Figure 9 shows the results obtained using these two algorithms.

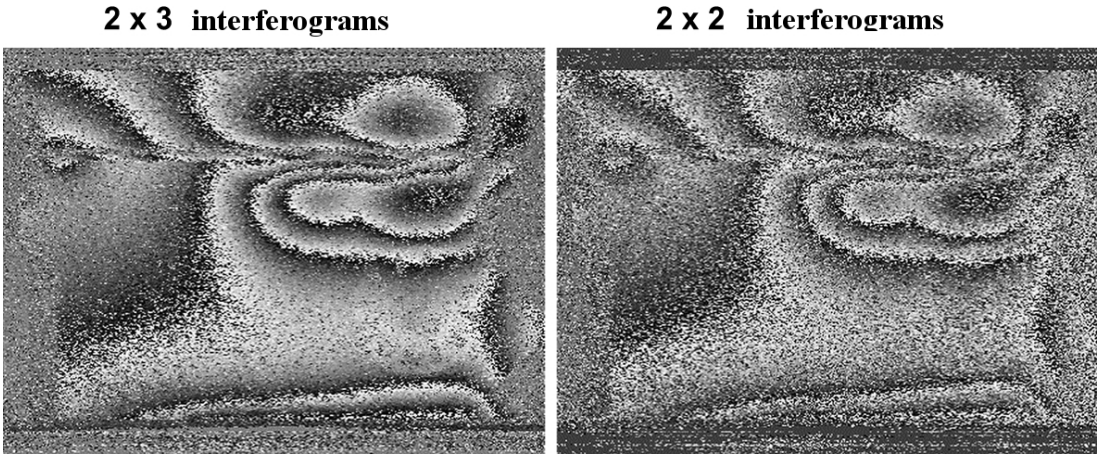

Figure 9 : Phase variation estimated with 2 X 2 and 2 X 3 interferograms

We clearly notice the direct influence of the number of interferograms, since the result obtained with 22 interferograms is noisier than with 23 interferograms, itself being noisier than the result obtained with 24 interferograms.

In speckle interferometry, the noise generated by speckle decorrelation while loading the object is the predominant source of noise.

In general, there are various sources of errors or fluctuations in the measurements made with interferometers, standard or speckle. These sources are listed in table 1.

Component	Origin of error	Classification
Laser	Average power variation	type B
	Coherence variation	type B
	Laser frequency variation	type B
	Shot noise	type A
Phase shifting	False calibration	type B
	Nonlinearity of the phase shift	type B
	Inequality of the phase shift	type A
Interferometer	Speckle decorrelation	type A
	Geometric aberrations	type B
	High-frequency vibration	type A
	Low-frequency vibration	type A
Detection	Electronic noise	type A
	Quantification noise	type A
	Non linearity	type B

Rappel

Uncertainties of type A : each source of uncertainty is studied by a statistical analysis performed on a series of observations and is characterized by its standard deviation, estimated using statistics.

Uncertainties of type B : the variance is estimated with a scientific judgment based on the available information related to the variability of the considered parameter.

The sensitivity of phase shifting algorithms to sources of systematic error and random fluctuations will be studied in the exercise section.

IV.Exercice

In the case study section, we highlighted various metrological aspects related to fringe pattern measurement. In particular, we showed how random fluctuations could alter phase measurements. However, even if decorrelation noise is predominant in speckle interferometry, for other applications other sources of noise can limit the demodulation resolution; one of them is shot noise. Among all sources of systematic errors listed in the table found in the case study section, we find the influence of incorrect shifting of interferograms.

1. Calculation of systematic errors

All error sources can be characterized using a parameter p, which generates an error in the estimation of phase $\Delta\varphi$. If we follow the recommendations of the GUM [16 [[16]]], the systematic error made on the phase can be estimated using the following equation:

$$\epsilon(\Delta\varphi,\phi,a,b,p)=\frac{\partial\Delta\varphi}{\partial p}dp+\frac{1}{2}\frac{\partial^2\Delta\varphi}{\partial p^2}(dp)^2+\ldots+\frac{1}{k!}\frac{\partial^k\Delta\varphi}{\partial p^k}(dp)^k+\ldots$$

Considering the general form of phase shifting algorithms, we can write [17 [[17]],18 [[18]]]

$$\Delta\varphi=\arctan\left(\frac{S(E_i)}{C(E_i)}\right)$$

It can be shown that $S(E_i)=\kappa\beta sin\Delta\varphi$ and $C(E_i)=\kappa\beta cos\Delta\varphi$, where κ is a coefficient which depends on the interferograms used for the calculation, and β relates to the parameter b of the fringe pattern.

The parameter p will introduce variations of $S(E_i)$ and $C(E_i)$, noted $dS(E_i)$ and $dC(E_i)$. In this case, the numerator and denominator will be equal to $\kappa\beta sin\Delta\varphi+dS(E_i)$ and $\kappa\beta cos\Delta\varphi+dC(E_i)$. The numerator and denominator variations induced by the parameter p will therefore give:

$$\varepsilon(\Delta\varphi,\phi,a,b,p)=\frac{\partial\Delta\varphi}{\partial S}dS(E_i)+\frac{\partial\Delta\varphi}{\partial C}dC(E_i)+\frac{1}{2}\frac{\partial^2\Delta\varphi}{\partial S^2}\left(dS(E_i)\right)^2+\frac{1}{2}\frac{\partial^2\Delta\varphi}{\partial C^2}\left(dC(E_i)\right)^2$$
$$+\ldots+\frac{1}{k!}\frac{\partial^k\Delta\varphi}{\partial S^k}\left(dS(E_i)\right)^k+\frac{1}{k!}\frac{\partial^k\Delta\varphi}{\partial C^k}\left(dC(E_i)\right)^k+\ldots$$

A linear approximation of this equation gives an approximate expression of the systematic error:

$$\varepsilon(\Delta\varphi,\phi,a,b,p)=\frac{\partial\Delta\varphi}{\partial S}dS(E_i)+\frac{\partial\Delta\varphi}{\partial C}dC(E_i)$$

This error can be characterized by its variance σ_ϵ which is estimated using the following relation [17 [[17]]] :

$$\sigma_\epsilon^2=\langle\epsilon^2(\Delta\varphi,\phi,a,b,p)\rangle-\langle\epsilon(\Delta\varphi,\phi,a,b,p)\rangle^2$$

with the *n* moment being equal to

$$\langle \epsilon^n(\Delta\varphi, \phi, a, b, p)\rangle = \int_{-\infty}^{+\infty} \epsilon^n(u, \phi, a, b, p) P_{\Delta\varphi}(u) du$$

and where $\langle ... \rangle$ indicates the statistical mean and $P_{\Delta\varphi}(\Delta\varphi)$ the probability density function of $\Delta\varphi$. We can consider that in the region of the fringes $\Delta\varphi$ is uniformly distributed on $[-\pi, +\pi]$. We therefore obtain:

$$\langle \epsilon^n(\Delta\varphi, \phi, a, b, p)\rangle = \frac{1}{2\pi}\int_{-\pi}^{+\pi} \epsilon^n(u, \phi, a, b, p) du$$

The peak to valley amplitude of $\epsilon(\Delta\varphi, \phi, a, b, p)$ is given by

$$PV_\epsilon = \max(\epsilon(\Delta\varphi, \phi, a, b, p)) - \min(\epsilon(\Delta\varphi, \phi, a, b, p))$$

2. Calculation of random errors

We consider a source of random error generating fluctuations on the interferograms; these fluctuations are random, uncorrelated, and of variance σ_E^2. By still referring to the GUM, the variance on the phase measurement corresponding to such a source of error can be expressed by:

$$\sigma_{\Delta\varphi}^2 = \sum_{i=1}^{i=N} \left(\frac{\partial \Delta\varphi}{\partial E_i}\right)^2 \sigma_{E_i}^2$$

This means that we simply have to sum the variances on each interferogram. We assumed that the fluctuations were random and (more importantly) uncorrelated between each image. Indeed, this simple relation does not take into account the correlations between variations. In practice, this assumption is often true.

The quantities $\frac{\partial \Delta\varphi}{\partial E_i}$ are called the **sensitivities of the algorithm**.

3. Description of the problem

In the case study section, we computed the phase with an algorithm using 4 images. The technical data are the same as in the case study.

We will consider the cases $b/a = 100\%$ and $b/a = 40\%$.

Review of mathematics

We remind the reader that

$$(f \circ g)'(x) = f'(g(x)) \times g'(x)$$

$$\arctan'(x) = \frac{1}{1+x^2}$$

Question 1

[*Solution n°1 p 54*]

Question 1 : Determine the sensitivities of the algorithm with 4 interferograms shifted by $\pi/2$

Question 2

[*Solution n°2 p 54*]

Question 2 : Determine the systematic error produced by a false calibration of the piezoelectric device; express its contribution to the phase measurement error, by estimating its standard deviation and its peak to valley amplitude.

Question 3

[*Solution n°3 p 55*]

Question 3 : In the case of speckle interferometry, what is the error on the phase? What can be deduce from this result?

Question 4

[*Solution n°4 p 55*]

Question 4 : Using the manufacturer data, evaluate the standard errors expressed in electrons for the shot noise (σ_p) and the quantization noise (σ_q)

Question 5

[*Solution n°5 p 56*]

Question 5 : Express the contributions of shot noise, quantization noise and electronic noise to the random error of the phase measurement

Solution des exercices

>Solution n°1 *(exercice p. 53)*

Since $\Delta\varphi = arctan\left(\frac{E_4 - E_2}{E_1 - E_3}\right)$, we have

$$\frac{\partial \Delta\varphi}{\partial E_1} = -\frac{E_4 - E_2}{(E_1 - E_3)^2}\frac{1}{1+\tan^2(\Delta\varphi)} = -\frac{1}{2b}\sin(\Delta\varphi)$$

$$\frac{\partial \Delta\varphi}{\partial E_2} = \frac{-1}{(E_1 - E_3)}\frac{1}{1+\tan^2(\Delta\varphi)} = -\frac{1}{2b}\cos(\Delta\varphi)$$

$$\frac{\partial \Delta\varphi}{\partial E_3} = \frac{E_4 - E_2}{(E_1 - E_3)^2}\frac{1}{1+\tan^2(\Delta\varphi)} = +\frac{1}{2b}\sin(\Delta\varphi)$$

$$\frac{\partial \Delta\varphi}{\partial E_4} = \frac{1}{(E_1 - E_3)}\frac{1}{1+\tan^2(\Delta\varphi)} = +\frac{1}{2b}\cos(\Delta\varphi)$$

>Solution n°2 *(exercice p. 53)*

The phase shifting must be produced with a value of

$$\phi = \frac{2\pi}{\lambda} s_{pzt} V$$

Considering that the value $spzt = 0.25\ \mu m/V$ is known with a precision of $\sigma_{pzt} = 5\%$, the difference between real and nominal shifts is $d\phi_i = (i-1)\phi\frac{\sigma_{pzt}}{s_{pzt}}$
The interferograms E_i are therefore

$$E_i = a + b\cos(\Delta\varphi + (i-1)\phi) - b(i-1)\phi\frac{\sigma_{pzt}}{s_{pzt}}\sin(\Delta\varphi + (i-1)\phi)$$

and the variation on the interferograms E_i is

$$dE_i = -b(i-1)\phi\frac{\sigma_{pzt}}{s_{pzt}}\sin(\Delta\varphi + (i-1)\phi)$$

We deduce that:

$$dS(E_i) = dE_4 - dE_2 = +\pi b\frac{\sigma_{pzt}}{s_{pzt}}\cos(\Delta\varphi)$$

$$dS(E_i) = dE_1 - dE_3 = -\pi\, b \frac{\sigma_{pzt}}{s_{pzt}} \sin(\Delta\varphi)$$

and the error on the phase measurement is:

$$\epsilon(\Delta\varphi, \phi, a, b, s_{pzt}) = \frac{\pi}{2} \frac{\sigma_{pzt}}{s_{pzt}} \cos(2\Delta\varphi)$$

We notice that the error has a periodicity equal to twice the periodicity of the fringe pattern variation, which means that the "fringe patterns of the error" have a step size twice smaller than the interferogram fringe pattern.
Using the mathematics of paragraph 2, we deduce the standard error:

$$\sigma_\epsilon = \frac{\pi}{2\sqrt{2}} \frac{\sigma_{pzt}}{s_{pzt}} = 0.055 \text{ rad} \approx \frac{2\pi}{113}$$

and the peak to valley amplitude:

$$PV_\epsilon = \max(\epsilon(\Delta\varphi, \phi, a, b, s_{pzt})) - \min(\epsilon(\Delta\varphi, \phi, a, b, s_{pzt}))$$

i.e.

$$PV_\epsilon = \pi \frac{\sigma_{pzt}}{s_{pzt}} = 0.157 \text{ rad} \approx \frac{2\pi}{40}$$

The calculated systematic error is on the order of 1/40th the fringe period. The precision is therefore not sufficient if we need a measurement with a precision better than 1/100th of the fringe period. On the other hand, the piezoelectric device is of sufficient quality for any application where the other sources of errors will impose larger limitations, as it is the case for example with speckle interferometry.

>Solution n°3 *(exercice p. 53)*

Considering that the phase is estimated by subtracting two individual phase measurements, we have

$$\epsilon(\Delta\varphi, \phi, a, b, s_{pzt}) = \frac{\pi}{2} \frac{\sigma_{pzt}}{s_{pzt}} \left(\cos(2\Delta\varphi + 2\psi) - \cos(2\psi)\right)$$

The error has a random nature due to the presence of the random phase in the above expression. Consequently, applying a digital filter to the phase map will strongly reduce this systematic error. Indeed, we saw that the correlation length of the speckle is on the order of one pixel. Therefore, its contribution in the measurement is most probably negligible.

>Solution n°4 *(exercice p. 53)*

The CCD sensor contains up to $30000 \text{ electrons per pixel}$ (at saturation). The corresponding shot noise is therefore equal to $\sigma_p = \sqrt{30000} = 173.2 \text{ electrons}$

The sensor digitizes the interferograms over $8\ bits$. The quantization step is therefore equal to $q \simeq \frac{30000}{2^8} = 117.64$ electrons and the standard error is equal to $\sigma_q = \frac{q}{\sqrt{12}} \simeq 34$ electrons.

>Solution n°5 *(exercice p. 53)*

For each noise source, the contribution to the random error of the optical phase measurement can be estimated using the following equation:

$$\sigma_{\Delta\varphi}^2 = \sum_{i=1}^{i=N} \left(\frac{\partial \Delta\varphi}{\partial E_i} \right)^2 \sigma_{E_i}^2$$

where $\sigma_{E_i} = \{\sigma_p, \sigma_e, \sigma_q\}$.
We assume that the noise is identical on each interferogram:

$$\sigma_{\Delta\varphi}^2 = \sigma_E \sum_{i=1}^{i=N} \left(\frac{\partial \Delta\varphi}{\partial E_i} \right)^2$$

with $\sigma_E = \{\sigma_p, \sigma_e, \sigma_q\}$
Using the previous expressions, we have

$$\sum_{i=1}^{i=N} \left(\frac{\partial \Delta\varphi}{\partial E_i} \right)^2 = \frac{1}{2b^2}$$

and:

$$\sigma_{\Delta\varphi} = \frac{\sigma_E}{\sqrt{2}b}$$

For each interferogram, the maximum value of E_i is equal to $a + b$ and the minimum value to $a - b$. Ideally, we would have $a = b$ and $2a = 30000\ electrons$. Therefore, we consider that $a = 15000\ electrons$
For the shot noise:

$$\sigma_{\Delta\varphi} = \frac{\sigma_p}{\sqrt{2}b} = \frac{1}{a} \times \frac{a}{b} \times \frac{173.2}{\sqrt{2}} = \frac{a}{b} \times 8.16 \text{ mrad}$$

$$\text{for} \quad b/a = 1 \qquad \sigma_{\Delta\varphi} = 8.16 \text{ mrad} \approx \frac{2\pi}{770}$$

$$\text{for} \quad b/a = 0.4 \qquad \sigma_{\Delta\varphi} = 20.4 \text{ mrad} \approx \frac{2\pi}{308}$$

For the electronic noise:

$$\sigma_{\Delta\varphi} = \frac{\sigma_e}{\sqrt{2}b} = \frac{1}{a} \times \frac{a}{b} \times \frac{10}{\sqrt{2}} = \frac{a}{b} \times 0.47 \text{ mrad}$$

$$\text{for} \quad b/a = 1 \qquad \sigma_{\Delta\varphi} = 0.47 \text{ mrad} \approx \frac{2\pi}{1336}$$

$$\text{for} \quad b/a = 0.4 \qquad \sigma_{\Delta\varphi} = 1.1 \text{ mrad} \approx \frac{2\pi}{571}$$

For the quantization noise:

$$\sigma_{\Delta\varphi} = \frac{\sigma_q}{\sqrt{2}\,b} = \frac{1}{a} \times \frac{a}{b} \times \frac{34}{\sqrt{2}} = \frac{a}{b} \times 1.6 \text{ mrad}$$

$$\text{for} \quad b/a = 1 \qquad \sigma_{\Delta\varphi} = 1.6 \text{ mrad} \approx \frac{2\pi}{3920}$$

$$\text{for} \quad b/a = 0.4 \qquad \sigma_{\Delta\varphi} = 1 \text{ mrad} \approx \frac{2\pi}{1568}$$

The shot noise is predominant, but has a much smaller contribution than the calibration error of the phase shifting device.

Bibliographie

[[01]] WYANT J.C., *Use of an ac Heterodyne Lateral Shear Interferometer With Real-Time Wavefront Correction Systems* (p.pp. 2622-2626), Applied Optics, 1975--, Vol. 14, n° 11, .

[[02]] BRUNING J.H., HERRIOTT D.R., GALLAGHER J.E., ROSENFELD D.P., WHITE A.D., BRANGACCIO D.J., *Digital Wavefront Measuring Interferometer for Testing Optical Surfaces and Lenses* (p.pp. 2693-2703), Applied Optics, 1974--, Vol. 13, n° 11, .

[[03]] GHIGLIA D.C., PRITT M.D., *Two-Dimensional Phase Unwrapping : Theory, Algorithms and Software*, Wiley Ed, New York, 1998.

[[04]] CREATH K., *Phase Measurement Interferometry Techniques* (p.pp 349-393), Progress in Optics - E. Wolf Ed., North-Holland publishing Company, 1988--, Vol. XXVI, .

[[05]] CARRE P., *Installation et Utilisation du Comparateur Photoélectrique et Interférentiel du Bureau International des Poids et Mesures,* (p.pp. 13-23), Metrologia, 1966--, Vol. 2, n° 1, .

[[06]] DORRIO B.V., FERNANDEZ J.L., *Phase Evaluation Methods in Whole-Field Optical Measurement Techniques* (p.pp 33-55), Measurement Science and Technology, 1999--, Vol. 10, .

[[07]] GREIVENKAMP J.E., *Generalized Data Reduction for Heterodyne Interferometry* (p.pp. 350-352), Optical Engineering, 1984--, Vol. 23, n° 4, .

[[08]] FRANTZ L.M., SAWCHUK A.A., OHE W., *Optical Phase Measurement in Real Time* (p.pp. 3301-3306), Applied Optics, 1979--, Vol. 18, .

[[09]] SCHWIDER J., BUROW R., ELSSNER K.E., GRZANNA J., SPOLACZYK R., MERKEL K., *Digital Wave-Front Measuring Interferometry : Some Systematic Error Sources* (p.pp. 3421-3432), Applied Optics, 1983--, Vol. 22, n° 21, .

[[10]] SASAKI O., OKAZAKI H., SAKAI M., *Sinusoidal Phase Modulating Interferometer Using the Integrating-Bucket Method ,* (p.pp. 1089-1093), Applied Optics, 1987--, Vol. 26, n° 6, .

[[11]] TAKEDA M., INA H., KOBAYASHI S., *Fourier-transform Method of Fringe-pattern Analysis for Computer-based Topography and Interferometry,,* (p.pp. 156-360), Journal of the Optical Society of America, 1982--, Vol. 72, n° 1, .

[[12]] KUJAWINSKA M., *The Architecture of a Multipurpose Fringe Pattern Analysis System* (p.pp. 261-263), Optics and Lasers in engineering, 1993--, Vol. 19, .

[[13]] WOMACK K.H, *Interferometric Phase Measurement Using spatial Synchronous Detection* (p.pp. 391-395), Optical Engineering, 1984--, Vol. 23, n° 4, .

[[14]] JONES R., WYKES C., *Holographic and speckle interferometry*, Cambridge University Press, Cambridge, 1989.

[[15]] CREATH K., *Phase Shifting Speckle Interferometry* (p.3053-3058), Applied Optics, 1985--, Vol. 24, n° 18, .

[[16]] - -, *Guide to the Expression of Uncertainty in Measurement*, ICS 03.120.30;17.020, GUM, -, June 1996.

[[17]] PICART P., *Error Analysis for a Mach Zehnder Type Speckle Interferometer* (p.pp. 335-353), Optics and Lasers in Engineering, 2001--, Vol. 35, n° 6, .

[[18]] PICART P., PASCAL J.-C., BRETEAU J.-M., *Systematic Errors of Phase Shifting Speckle Interferometry* (p.2107-2116), Applied Optics, 2001--, Vol. 40, n° 13, .